Performance evaluation of IEC 60891:2021 procedures for correcting I – V curves of photovoltaic modules under healthy and faulty conditions

Baojie Li, Demba Diallo, Anne Migan-Dubois, Claude Delpha

Received: 11 February 2022 | Revised: 30 October 2022 | Accepted: 7 November 2022

DOI: 10.1002/pip.3652

RESEARCH ARTICLE

PROGRESS IN PHOTOVOLTAICS WILEY

Performance evaluation of IEC 60891:2021 procedures for correcting *I–V* curves of photovoltaic modules under healthy and faulty conditions

Baojie Li[1,2] | Demba Diallo[1] | Anne Migan-Dubois[1] | Claude Delpha[2]

[1]Université Paris-Saclay, CentraleSupélec, CNRS, GeePs, Sorbonne Université, 3-11 Rue Joliot Curie, Gif Sur Yvette, 91192, France

[2]Université Paris-Saclay, CNRS, CentraleSupélec, L2S, 3 Rue Joliot Curie, Gif Sur Yvette, 91192, France

Correspondence
Demba Diallo, Université Paris-Saclay, CentraleSupélec, CNRS, GeePs, Sorbonne Université, 3-11 Rue Joliot Curie, Gif Sur Yvette 91192, France.
Email: demba.diallo@centralesupelec.fr

Abstract

Correction of PV modules' current–voltage characteristics (*I–V* curves) is essential before they can be used for performance analysis and fault diagnosis under real-life conditions. IEC 60891 (version 2021) has updated Procedure 2 and proposed a new correction Procedure 4 compared to the 2009 version. This study aims to analyze the performance of these new procedures applied to *I–V* curves of faulty PV modules. The work is based on an mc-Si PV module considering healthy and four common fault conditions with varying fault severity. The irradiance and temperature measured in the field are used to generate *I–V* curves. The correction procedures of IEC 60891 (version 2021) based on a single curve (Procedures 1, 2, and 4) are evaluated. Environmental factors such as measurement season and irradiation level on the correction performance are studied. The results show that Procedure 2 is relatively better with the relative root-mean-square error of the curve current as 2.6% compared to Procedure 1 (2.8%) and Procedure 4 (4.8%). Experimental tests using real *I–V* curves also show that Procedure 2 exhibits better robustness of correction. The new Procedure 4, whose correction coefficients are determined dynamically, performs poorly under partial shading and short-circuit bypass conditions. However, it achieves similar or better performance than Procedures 1 and 2 under degraded conditions, where the PV fault is generally not easy to detect, making the *I–V* correction more necessary. It is, therefore, a promising alternative correction procedure when it is difficult to determine the correction coefficients in advance. Finally, the pros and cons of the procedures are discussed with the suggestion of correction procedures under different conditions. The challenges and prospects are also provided.

KEYWORDS
correction performance, fault diagnosis, IEC 60891, *I–V* curve, PV modules

1 | INTRODUCTION

The current–voltage characteristics (*I–V* curves) contain much information about the health of a photovoltaic (PV) module or array.[1,2] Typically, *I–V* curves under various environmental conditions are measured by *I–V* tracing devices for a PV module or small-scale PV array.[3,4] In recent years, hardware solutions (integrated into inverters)[5] have been commercialized to record *I–V* curves for a large-scale array or power plant.[6,7] With the increasing availability of *I–V* curves on-site, monitoring and maintaining PV modules using *I–V* curves is gaining more and more research interest.[8,9] However, because of the sensitivity of the *I–V* curve to the environmental conditions, the IEC 60891 proposed several standard procedures to correct *I–V* curve before the comparison of *I–V* characteristics measured under different environmental conditions. Generally, standard test condition (STC) is the target condition.[1] After the correction, the whole curve or the key curve parameters are used for health monitoring or fault diagnosis.[2] Specifically, the open-circuit voltage (V_{OC}), short-circuit current (I_{SC}), the voltage at the point of maximum power (V_{MPP}), current (I_{MPP}), and power (P_m) can be extracted for fault diagnosis[3–5] or power loss analysis.[6] Additionally, the equivalent series resistance (R_s) or shunt resistance (R_{sh}) are commonly computed for long-term performance[7] or degradation analysis of PV devices.[8,10]

In this respect, if the corrections cause errors in the corrected curves or the curve parameters, monitoring or diagnostic performance will be impaired. Therefore, the accuracy of the *I–V* curve correction is essential.

IEC 60891 (version 2009)[9] standard proposed three correction procedures, which have been widely applied for the correction of *I–V* curves measured from healthy or faulty PV devices.[11,12] For example, Procedure 1 of IEC 60891 (version 2009) is used to correct *I–V* curves measured under partial shading (PS),[13,14] hot spot,[15] dust soiling,[16,17] or for degradation analysis[18–20] or power rating.[21] Procedure 2 (version 2009) is employed to correct the key *I–V* curve parameters.[4] These corrected parameters could then be used as inputs to different tools[22] (e.g., artificial neural network, support vector machine, and decision tree) to classify the different defects.[11,23] In Kumar and Maheshwari,[24] Procedure 2 is applied with the corrected *I–V* curves correlated with PV electroluminescence (EL) images to identify defects in EL images. In Ayang et al.,[25] both Procedures 1 and 2 are also explored for the estimation of single-diode model parameters. In addition to the application of procedures, some research focused on the mechanism of the correction procedures. Dobreva et al.[26] show that the nature of the translation is the affine transformations of concave functions on convex sets. Duck et al.[27] investigated the correction performance at varying irradiance and temperature. Similar work is performed by Haas et al.,[28] Tsuno and Hishikawa,[29] and Raina et al.[22] (focusing on the modified Procedure 2). Hishikawa et al.[37] explored Procedure 3 using wide-range linear extrapolation under different weather conditions. Padilla et al.[30] tested Procedure 3 for PV modules of different technologies. Paudyal and Imenes[31] studied the temperature coefficient estimated by the correction procedures. Besides, various modified versions of correction procedures have been proposed. Ding et al.[32] proposed an improved Procedure 2 to simplify the modeling of PV modules. A modified Procedure 1 is introduced by Golive et al.[33] on neglecting two correction coefficients. Abe et al.[34] ameliorate the determination of the correction coefficients of Procedure 2 by reducing the number of required *I–V* curves.

Recently, the 2021 version of the IEC 60891 was released.[35] It updates Procedure 2 (based on Pingel et al.'s research[36]) and introduces a new Procedure 4 (based on Hishikawa et al.'s research[37]), while Procedures 1 and 3 remain unchanged. Although this version is new, some researchers have focused on the procedures. Golive et al[38] evaluated the sensitivity of Procedures 1, 2, and 4 to the temperature coefficients. It is suggested that Procedure 4 is less sensitive to the error on temperature coefficient. Piliougine et al.[39] have selected Procedure 3 for the degradation analysis of PV modules after long-term operation.

It is noteworthy that both versions of IEC 60891 standard are all initially designed for the *I–V* curves of healthy PV devices. Therefore, the previous work[40,41] has studied the correction performance of procedures in IEC 60891:2009 when dealing with *I–V* curves of defective PV modules. It was pointed out that all the procedures are prone to introduce large distortion to the shape of the curve and the related curve parameters after correction. However, the research is still limited as only high irradiance and high module temperature have been considered. Besides, the new procedures in the 2021 version have not yet been discussed for the correction of *I–V* curves of faulty PV modules.

This paper aims to fill this gap by making the following contributions:

- The correction procedures in IEC 60891 (version 2021) are firstly evaluated with *I–V* curves of the PV module under both healthy and faulty conditions.
- The impacts of environmental factors, the season of measurement, and the irradiance level on the correction performance are investigated in detail.
- The correction performance with *I–V* curves under four typical faulty conditions is studied with varying fault severities.
- Limits of each correction procedure are identified, and suggestions are given on the selection of correction procedures under different conditions.

The remainder of the paper is organized as follows. Section 2 presents the evaluation's methodology, including the generation of faulty *I–V* curves, the correction procedures, and the evaluation metrics. The correction performance is detailed in Section 3 while addressing the impact of environmental factors for four typical case studies. A summary of the correction procedures, challenges, and prospects is provided in Section 4. Section 5 concludes the study.

2 | METHODOLOGY FOR THE EVALUATION OF CORRECTION PROCEDURES

As the purpose of the research is to examine the errors due to the correction procedures, it is necessary to remove the impact of all

other uncertainty factors, especially the measurement errors of the irradiance, the temperature, and the *I*–*V* curve, which could reach more than 5%.[33] Therefore, the curves to correct are recorded from simulation instead of field measurements.

2.1 | Generation of *I*–*V* curves

2.1.1 | Simulation model of the PV module

To simulate different fault types, a 305 W PV mc-Si module (Q.PEAK-G4-305) is modeled under Matlab Simulink®, as illustrated in Figure 1. The module comprises 60 cells connected in series and three bypass diodes (each bypasses 20 cells). The module V_{OC} is 40.1 V, and I_{SC} 9.84 A.

The PV cell is modeled based on the common equivalent circuit model—single-diode model[42] shown in Figure 2. This model contains five parameters, that is, the photocurrent (I_{ph}), saturation current (I_o), series resistance (R_s), shunt resistance (R_{sh}), and the modified diode factor (a). The fundamental relationship between V and I is described in 1.

$$I = I_{ph} - I_0\left[\exp\left(\frac{V+IR_s}{a}\right)-1\right]-\frac{V+IR_s}{R_{sh}}. \quad (1)$$

The five irradiation- and temperature-dependent parameters are estimated using Model 2 proposed in Golive et al.[33] (detailed in Section A of the Supporting Information), which was found to be the most efficient among the current candidate models for modeling the experimental *I*–*V* curves.[33]

Using the presented module model, five conditions of the PV module are addressed, that is, the healthy condition and four typical faults:

- PS: One third of the module surface is shaded by adjusting the PS degree
- Short-circuit bypass diode (SC BPD): One bypass diode is short-circuited by adding resistance R_{SC} in parallel
- Rs degradation (Rs degra): Resistance R_{s_degra} is added in series to control the equivalent series resistance
- Rsh degradation (Rsh degra): Resistance R_{sh_degra} is added in parallel to control the equivalent shunt resistance

The setting of fault parameters for the five module conditions is detailed in Table 1. Examples of the *I*–*V* curves at STC ($G = 1000$ W/m^2 and $Tm = 25$°C) under these conditions are illustrated in Figure 3. It should be noted that, for PS, Rs, and Rsh degradation, the fault severity could vary in the range presented in Table 1. The used values will be detailed in Section 3.

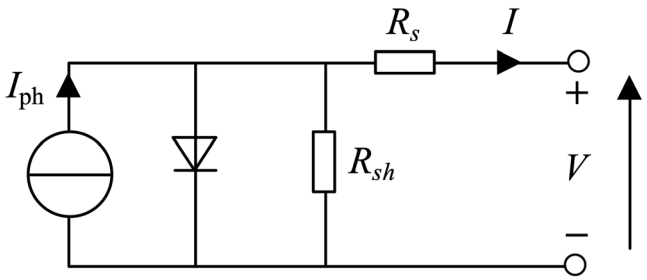

FIGURE 2 Desoto single-diode PV cell model

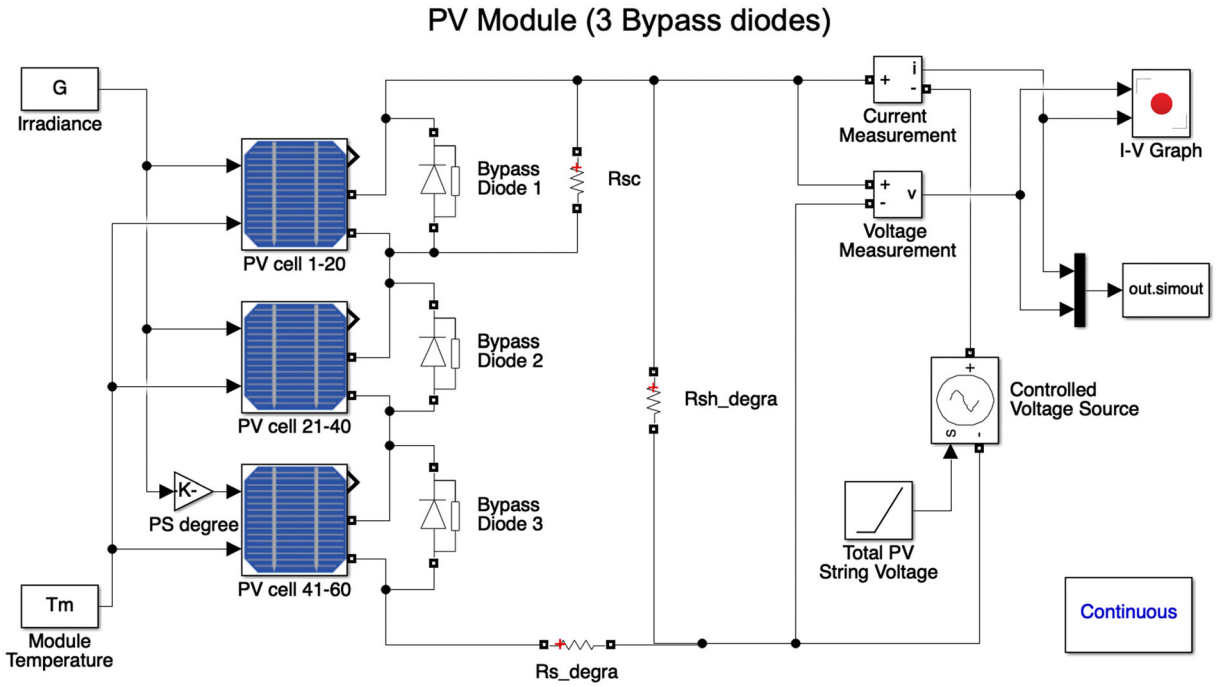

FIGURE 1 Simulation model of the PV module [Colour figure can be viewed at wileyonlinelibrary.com]

Condition	PS degree (%)	R_{SC} (Ω)	R_{OC} (Ω)	R_{s_degra} (Ω)	R_{sh_degra} (Ω)
Healthy	0	10^5	10^{-5}	10^{-5}	10^5
PS	**0–100**	10^5	10^{-5}	10^{-5}	10^5
SC BPD	0	**10^{-5}**	10^{-5}	10^{-5}	10^5
Rs degradation	0	10^5	10^{-5}	**[10^{-5}–2]**	10^5
Rsh degradation	1	10^5	10^{-5}	10^{-5}	**[10^5–10]**

Note: The bold type is used to point out the range of variation to emulate each fault type.

TABLE 1 Parameter setting for the different conditions

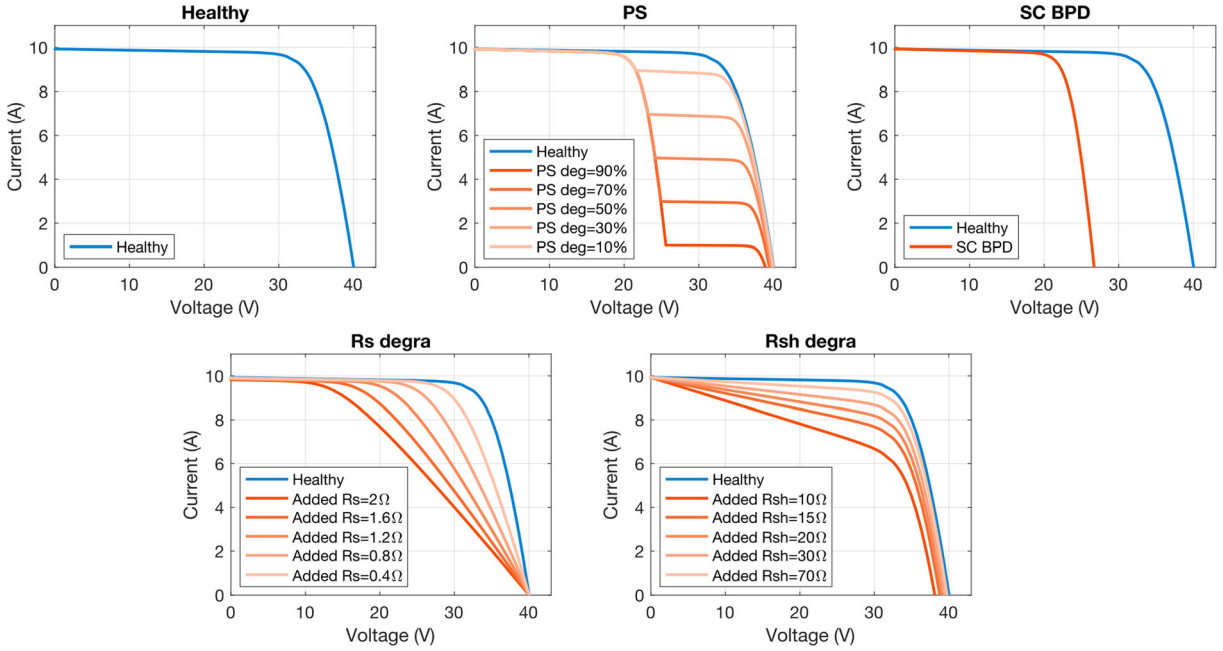

FIGURE 3 Examples *I*–*V* curves of the PV module under five conditions at STC [Colour figure can be viewed at wileyonlinelibrary.com]

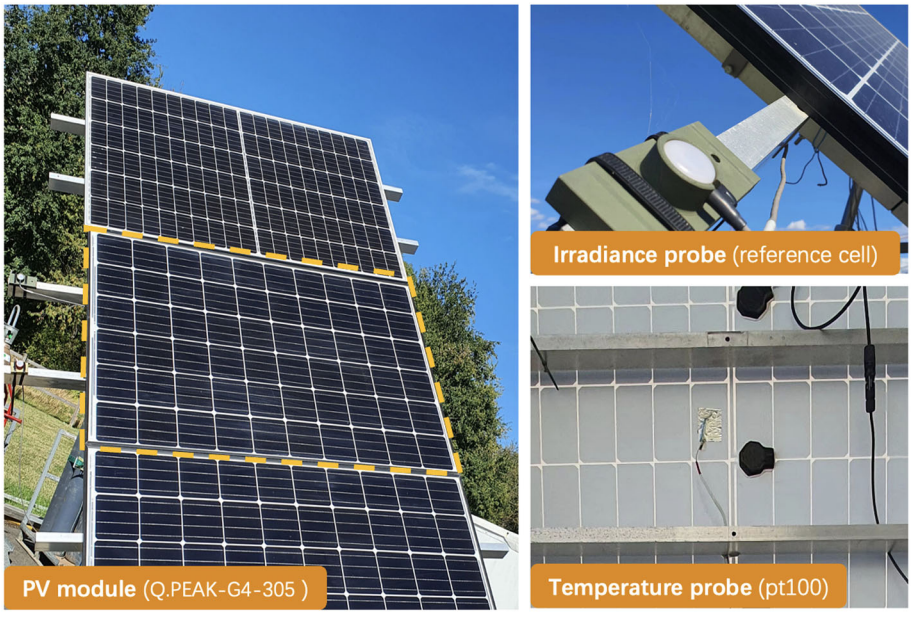

FIGURE 4 Configuration of PV module measurement [Colour figure can be viewed at wileyonlinelibrary.com]

2.1.2 | Validation of the simulation model using real *I*–*V* curves

To validate the simulation model, the simulated and real-measured *I*–*V* curves of the same PV module (Q.PEAK-G4-305) are compared. The field measurement configuration is shown in Figure 4. Due to the tested module being in continuous operation, only the *I*–*V* curves under healthy conditions are used for the test. The curves cover a wide-range *G* (200–1200 W/m^2) with the examples presented in Figure 5. To quantify the matching degree, the root-mean-square error (RMSE) between the current of the simulated and real *I*–*V* curve is calculated. The average relative RMSE (normalized by the module short-circuit current) is 0.42% and the mean correlation coefficient reaches 0.99, which both demonstrate the good performance of the simulation model. In addition, Golive et al.[33] have also proved that the adopted SDM model in Section 2.1.1 better fits the experimental *I*–*V* curves and is more suitable to generate simulated *I*–*V* curves for correction analysis.

2.2 | Correction procedures in IEC 60891:2021

IEC 60891:2021[35] provides four procedures for correcting the *I*–*V* curve. Compared to the 2009 version,[9] a new procedure (Procedure 4) has been added, and the original Procedure 2 has been updated. Procedures 1 and 3 have not been changed. Procedures 1, 2 and 4 are based on a single *I*–*V* curve to be corrected, while Procedure 3 requires at least three reference *I*–*V* curves at different *G* and *Tm* for the STC correction. It should also be noted that Procedures 1 and 2 require multiple *I*–*V* curves at identical *G* or *Tm* to extract the correction coefficients.[35] Since Procedure 3 is different from the others and its correction performance has already been evaluated in previous work,[40] this research focuses on the single curve-based correction procedures, that is, Procedures 1, 2 and 4, which are briefly presented below.

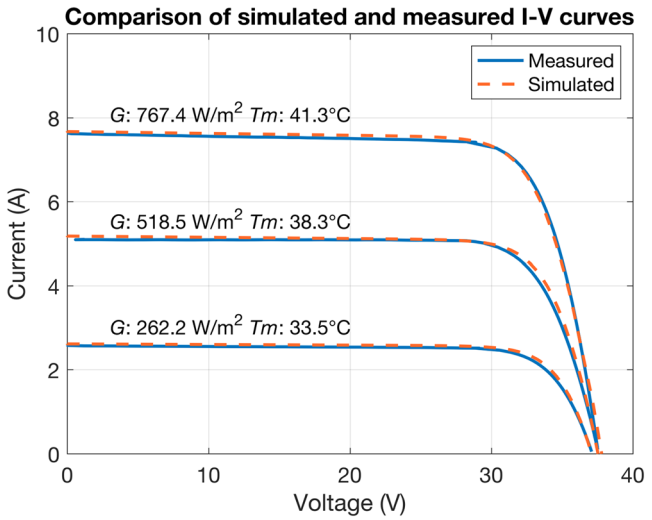

FIGURE 5 Examples of measured and simulated (using the model in Figure 1) *I*–*V* curves [Colour figure can be viewed at wileyonlinelibrary.com]

- Procedure 1 (P1):

$$I_2 = I_1 + I_{SC1}(G_2/G_1 - 1) + \alpha(T_{m2} - T_{m1}), \tag{2}$$

$$V_2 = V_1 - R_s(I_2 - I_1) - \kappa I_2(T_{m2} - T_{m1}) + \beta(T_{m2} - T_{m1}), \tag{3}$$

where I_1 and I_2, V_1 and V_2, T_{m1} and T_{m2}, and G_1 and G_2 are the current, voltage, module temperature, and irradiance before and after correction, respectively; I_{SC1} is the short-circuit current before correction; α and β are the PV module absolute temperature coefficient (TC) of I_{SC} and V_{OC}, respectively; $\alpha = \alpha_{rel} \cdot I_{SC}^{STC}$, $\beta = \beta_{rel} \cdot V_{OC}^{STC}$, and α_{rel} and β_{rel} are the relative TC of I_{SC} and V_{OC}; V_{OC}^{STC} and I_{SC}^{STC} are the V_{OC} and I_{SC} at STC, respectively, provided in the module datasheet; R_s is the internal series resistance; and κ is the curve correction factor.

- Procedure 2 (P2):

$$I_2 = I_1 \frac{G_2\,(1 + \alpha_{rel}(T_{m2} - 25))}{G_1\,(1 + \alpha_{rel}(T_{m1} - 25))}, \tag{4}$$

$$\begin{aligned} V_2 = {} & V_1 - R'_{s1}(I_2 - I_1) - \kappa' I_2(T_{m2} - T_{m1}) \\ & + V_{OC}^{STC}\left\{\beta_{rel}[f(G_2)(T_{m2} - 25) - f(G_1)(T_{m1} - 25)] + \frac{1}{f(G_2)} - \frac{1}{f(G_1)}\right\}, \end{aligned} \tag{5}$$

$$f(G) = B_2 \cdot \ln(1000/G)^2 + B_1 \cdot \ln(1000/G) + 1, \tag{6}$$

$$R'_{s1} = R'_s + \kappa'(T_{m1} - 25), \tag{7}$$

where R'_s is the resistance at 25°C while R'_{s1} is at T_{m1}. κ' is the TC of R'_s; $f(G)$ is a quadratic irradiance-dependent factor accounting for the diode ideality factor. B_1 and B_2 are the irradiance correction factors.

For P1 and P2, the coefficients R_s, R'_s, κ, κ', B_1, and B_2 are determined by using a group of simulated *I*–*V* curves at the same *G* or same *Tm*.[35] For this research's PV module (Q.PEAK-G4-305), the extracted correction coefficients for P1 and P2 are listed in Table S1. Additionally, in field applications, it is generally challenging to know the exact health condition of one PV module and the corresponding correction coefficients. Therefore, the predetermined parameters are adopted for all the case studies.

- Procedure 4 (P4):

Different from P1 and P2, P4 does not require prior-determined correction coefficients. It requires only the bandgap ε of the module material and the number of cells in series (n_s). n_s is the number of cells in series of the module.

$$I_1' = I_1 + I_{sc1}\left(\frac{G_2}{G_1} - 1\right), \tag{8}$$

$$V_1' = V_1 - R_s(I_1' - I_1), \tag{9}$$

$$I_2 = I_1' + \alpha_{rel} I_{sc}^{STC}(T_{m2} - T_{m1}), \tag{10}$$

$$V_2 = V_1' + \frac{(T_{m2} - T_{m1})}{T_{m1}}(V_1' - n_s \times \varepsilon). \tag{11}$$

R_s in 8 can be determined by the curve to correct based on an analysis of a group of points from the high-voltage region of the *I*–*V* curve, as detailed in IEC 60891.[35] $(V_1' - n_s \times \varepsilon)$ is a voltage-dependent temperature coefficient (VDTC),[43] which, different from β_{rel} adopted in P1 and P2, also depends on the voltage. ε is a constant depending on the PV device (in units of V). For c-Si, it is recommended to be 1.232 V.[35]

Since STC is more commonly adopted as the target condition for *I*–*V* curve-based analysis, in the following, if not stated, the correction of *I*–*V* curves refers to the correction to STC.

2.3 | Metrics for the evaluation of correction performance

The correction performance will be quantified from the RMSE of the curve current and relative error (*RE*) of key curve parameters. The *RE* is expressed as

$$RE_X = \frac{X^c - X^{ref}}{X^{ref}} \times 100\%, \tag{12}$$

where X^c and X^{ref} are the parameters of the corrected and reference curve, respectively. *X* can be P_m, V_{OC}, I_{SC}, or the fill factor (FF).

Indeed, the nature of the correction process could be considered as the "inverse" of the simulation function. Thus, the correction procedure closest to the simulation model is supposed to achieve better performance. Actually, Procedures 1, 2, and 4 are all based on the same single-diode model.[35,37] However, due to the solution to the fundamental function 1 of the single-diode model is not algebraically solvable, which is also true for the "inverse" of the model, different assumptions and simplifications are introduced in the procedures. For example, Procedure 1 assumes that diode current is independent of photocurrent, Procedure 2 considers a quadratic relationship between the diode factor with the irradiance, and Procedure 4 neglects the shunt resistance. Therefore, our work is to evaluate the correction performance of these procedures and to see the trade-off between the assumptions/simplifications and the correction performance under the different circumstances (various fault, environmental factors, and fault severity), all of which will be detailed in the next section.

3 | CORRECTION PERFORMANCE

The environmental parameters (*G* and *Tm*) significantly affect the form of an *I*–*V* curve, which determines the correction performance. Seen in this light, Section 3.1 investigates the impact of *G* and *Tm* on the correction performance under five PV module conditions using the three procedures. The trends of the errors will be analyzed. Since the field-measured studied *G* and *Tm* generally do not fully cover the range given in Section 3.1, Section 3.2 presents four common case studies, which provide a quantitative analysis of the performance focusing on the range of *G*, the season of measurement, and the fault severity. Lastly, preliminary tests of the correction procedures using experimental *I*–*V* curves will be presented.

3.1 | Impact of irradiance *G* and temperature *Tm*

To investigate the impact of *G* and *Tm*, the fault severity is firstly set constant with typical values, as defined in Table 2. Corresponding *I*–*V* curves under STC refer to Figure 3.

For the environmental conditions, *G* varies from 100 to 1200 W/m^2 while *Tm* varies from 0°C to 70°C. The *I*–*V* curves under these environmental configurations and the five PV module conditions are corrected to STC by using P1, P2, and P4. The heatmap of the correction RMSE, examples of corrected curves, and correction error of key curve parameters (RE_{P_m}, $RE_{V_{OC}}$, $RE_{I_{SC}}$, and RE_{FF}) under healthy, PS, SC BPD, Rs degradation, and Rsh degradation are illustrated in Figures 6–11, respectively.

When the module is under healthy condition, based on the RMSE heatmap, intuitively, it is observed that P2 achieves better correction than P1 and P4. This is also reflected in the corrected *I*–*V* curves in Figure 6b and the key parameters Figure 6c, where the corrected curves coincide better with the reference curve (simulated at STC). For P1, the lower RMSE is observed for a condition close to STC while a large RMSE occurs for low *G*. For P2, lower RMSE is observed for low *Tm*, especially around 25°C. For P4, the correction is efficient around the STC condition. However, when the *G* and *Tm* get far from the STC, the performance deteriorates more significantly compared to P1 and P2. This is mainly due to two factors. First, the coefficient R_s used for the correction should be close to the module internal R_s. However, the value used in P4, which is dynamically determined, deviates from the proper value (internal R_s) with decreasing *G* as shown in Figure 7, compared to the constant value (close to the internal R_s) in P1 and P2. Second, a missing temperature correction coefficient in P4

TABLE 2 Fault severity setting

Condition	Fault severity
PS	PS degree = 50%
Rs degradation	$R_{s\_degra} = 0.5\ \Omega$
Rsh degradation	$R_{sh\_degra} = 20\ \Omega$

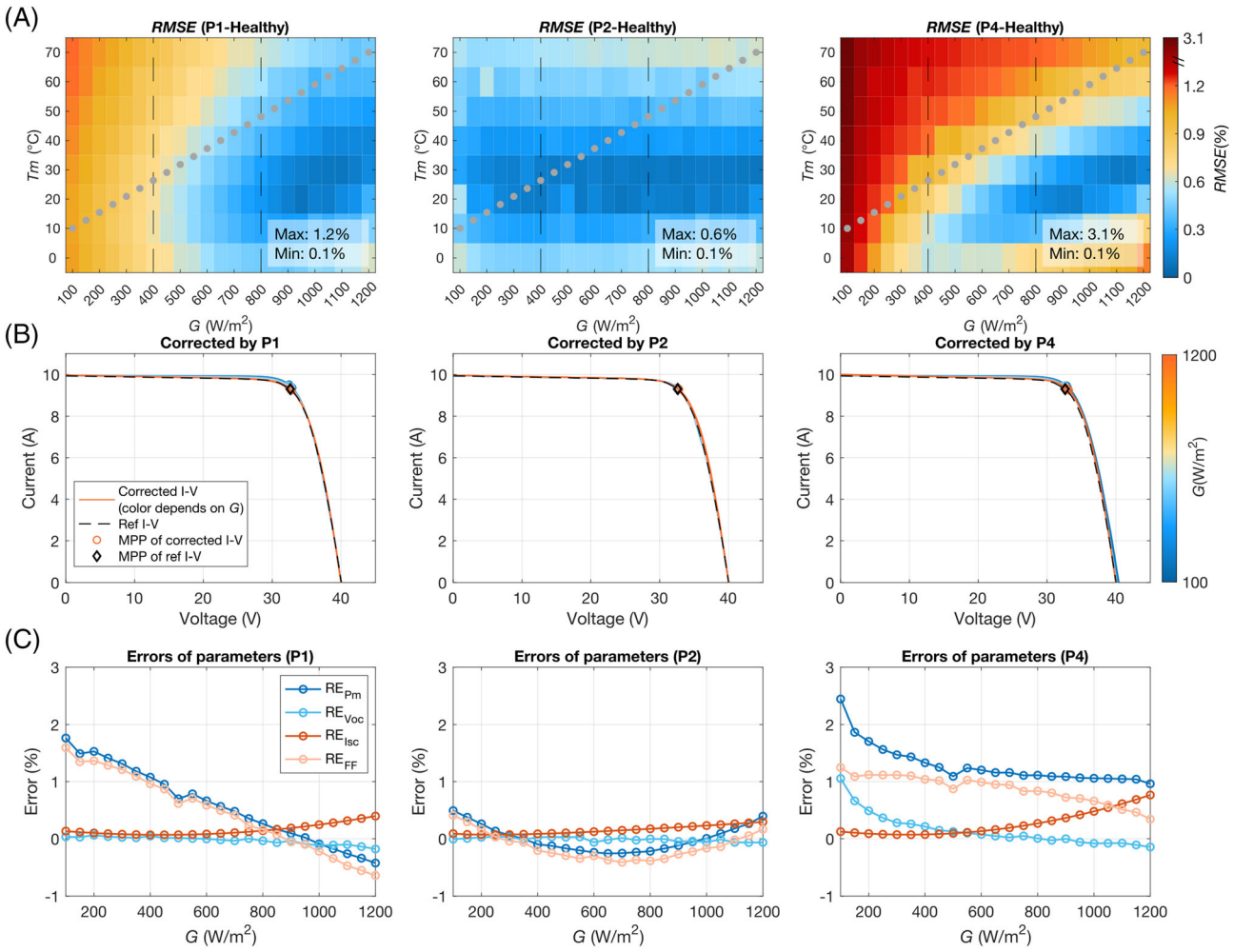

FIGURE 6 (A) Heatmap for the RMSE of the correction of *I*–*V* curves under the healthy condition using P1, P2, and P4 (gray points represent the *G* and *Tm* of example *I*–*V* curves, where the corrected ones and the errors of parameters are shown in (B) and (C), respectively); (B) examples of corrected *I*–*V* curves under healthy condition; and (C) errors of key parameters from the examples of corrected *I*–*V* curves [Colour figure can be viewed at wileyonlinelibrary.com]

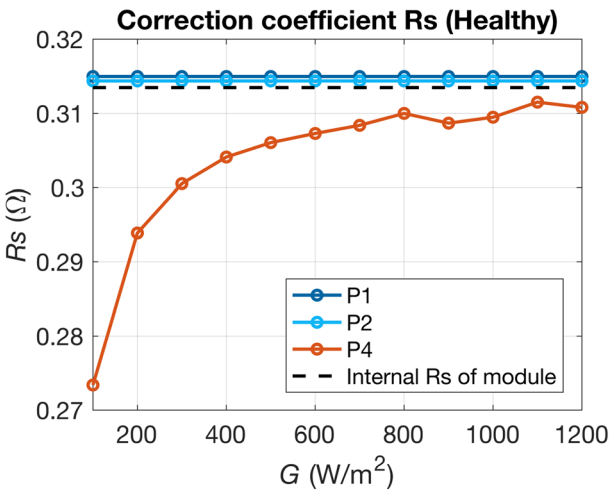

FIGURE 7 Correction coefficient Rs used in P1, P2, and P4 (extracted from *I*–*V* curves at 25°C and varying *G*) [Colour figure can be viewed at wileyonlinelibrary.com]

leads to a higher error at high *Tm*. Therefore, the correction performance of P4 is less satisfying than P1 or P2.

In terms of the curve parameters, for P1, RE_{P_m} is observed more sensitive to the varying *G* than $RE_{V_{OC}}$ and $RE_{I_{SC}}$, which consequently affects the RE_{FF}. Similar trends are also noted for P4. Comparatively, the parameter using P2 are more stable with the *RE* within ±1%.

Regarding PS, for P1 and P4, the impact of irradiance *G* on RMSE heatmap is more dominant compared to *Tm*. Lower *G* leads to higher RMSE. For all the procedures, large correction errors are observed in the region around the reflection point. For P4, additional significant errors occur in the region near V_{OC}. To look into these correction errors, the following analysis is performed from the correction of current (reflected along the *y* axis) and the voltage (along the *x* axis), respectively. P1 and P4 have close current correction equations, which are notably different from that of P2: The correction is independent of the short-circuit current, and the current after correction (I_2) is proportional to the one before correction (I_1). Consequently, we observe that P1 and P4 introduce large errors in the current

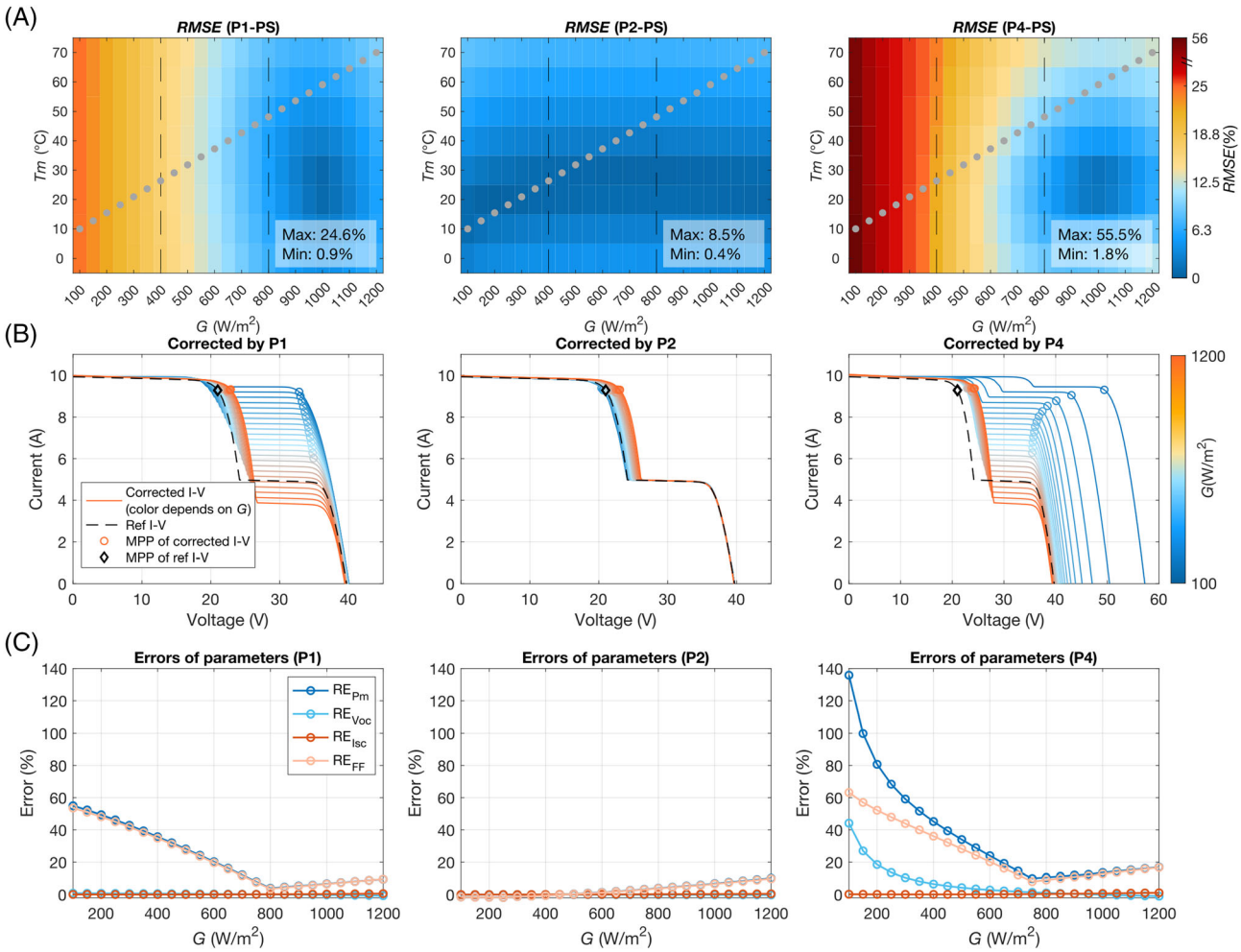

FIGURE 8 (A) Heatmap for the RMSE of the correction of *I*–*V* curves under PS using P1, P2, and P4 (gray points represent the *G* and *Tm* of example *I*–*V* curves, where the corrected ones and the related errors of parameters are shown in (B) and (C), respectively); (B) examples of corrected *I*–*V* curves under PS; and (C) errors of key parameters from the examples of corrected *I*–*V* curves [Colour figure can be viewed at wileyonlinelibrary.com]

correction near the reflection point, which leads to the large RE_{P_m} (up to 140%) and RE_{FF} (up to 61%) as shown in Figure 8C. For P1 and P2, there is a significant voltage correction error near the reflection point. It is because the improper V_{OC} is used to correct part of the curve voltage where the V_{OC} is decreased due to the activation of bypass diode, which also causes the change of the curve slope near the V_{OC} region (as illustrated in Figure 3 compared to the healthy curve). This leads to the catastrophic error in the voltage correction for P4, which relies on the curve near the V_{OC} region to dynamically extract the coefficient R_s for correction. This bias on R_s is even aggravated with lower *G*, as shown in Figure 7 and reflected from the $RE_{V_{OC}}$ in Figure 8C. This poor performance of Procedure 4 is also mentioned in IEC 60891:2021,[35] where it is stated that Procedure 4 is probably not applicable when the PV device is affected by PS.

For SC, the symmetry of RMSE heatmap is similar for the three procedures. RMSE is more affected by the temperature *Tm* than the irradiance *G*. Large errors appear in the voltage correction, affecting both the $RE_{V_{OC}}$ and RE_{FF}. These errors are due to improper voltage correction coefficients used in 3, 5, and 11. Indeed, they are set in healthy conditions, whereas, with one BPD short-circuited, the module V_{OC} is severely reduced.

In the case of series resistance Rs degradation, the irradiance *G* is also the dominant factor compared to *Tm*. Significant correction error is introduced in the MPP region (reflected from RE_{P_m} and RE_{FF}) when using P1 and P2, because the used coefficient R_s (constant value) does not reflect the change of the module R_s under Rs degradation. Comparatively, P4 calculates the R_s dynamically. Thus, when the irradiance *G* is high, a stable extraction of R_s leads to a better correction. As for the $RE_{V_{OC}}$, P1 results in large errors than P2. It is because the irradiance *G* is not taken into account in the voltage correction, as it can be observed in 3 and 5.

Under Rsh degradation conditions, for P1 and P4, the temperature *Tm* is more influential, in contrast to P2 for which it is the irradiance whose low values considerably degrade the correction. This is mainly due to the fact that the current correction for P1 and P4 takes into account the irradiance through the short-circuit current.

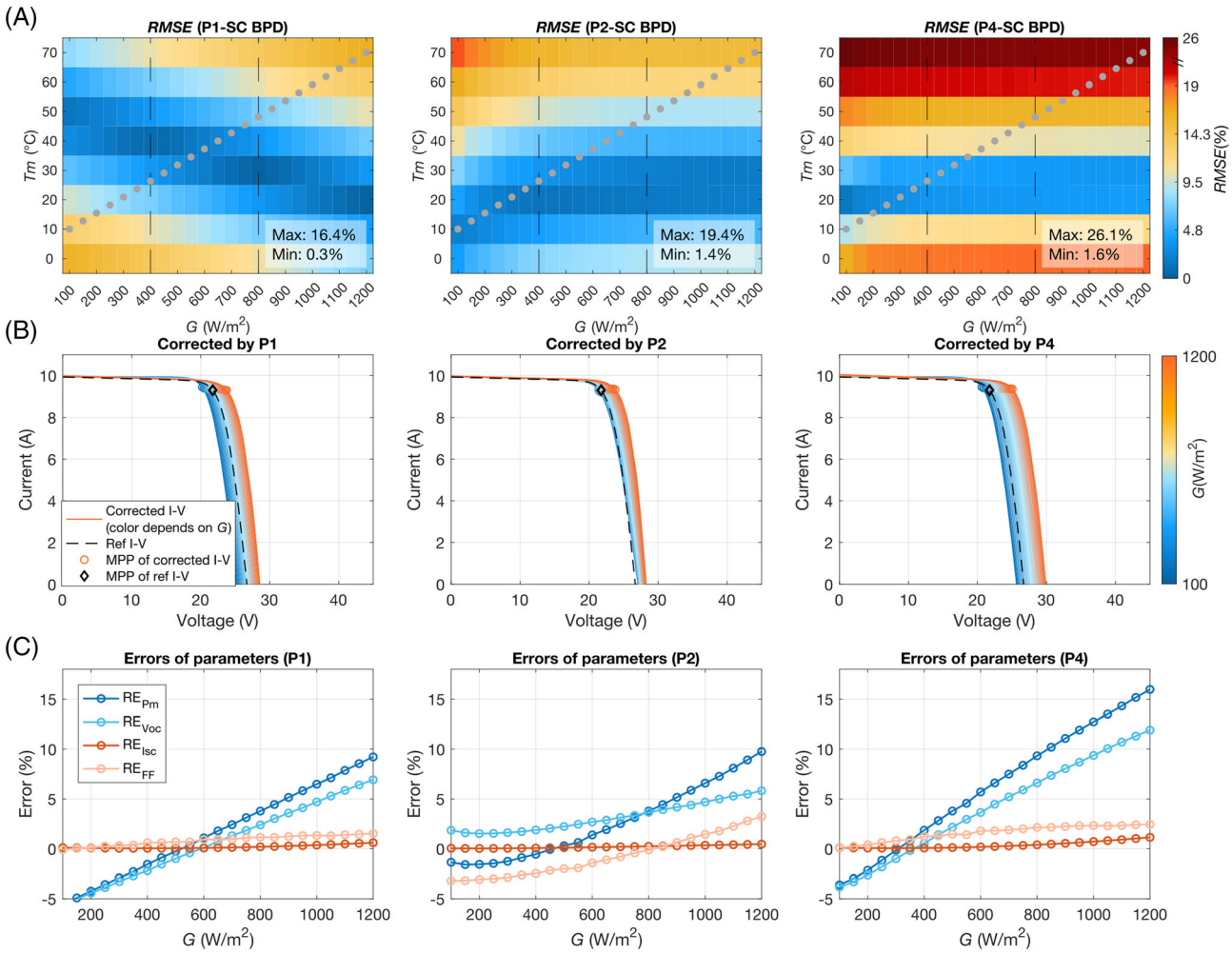

FIGURE 9 (A) Heatmap for the RMSE of the correction of *I*–*V* curves under SC BPD using P1, P2, and P4 (gray points represent the *G* and *Tm* of example *I*–*V* curves, where the corrected ones and the related errors of parameters are shown in (B) and (C), respectively); (B) examples of corrected *I*–*V* curves under SC BPD; and (C) errors of key parameters from the examples of corrected *I*–*V* curves [Colour figure can be viewed at wileyonlinelibrary.com]

Therefore, as the irradiance decreases (so does the current), the correction of P2 is less efficient compared to P1 and P4, especially near MPP region (reflected from RE_{P_m} and RE_{FF}). This effect is attenuated near high-voltage region as the current contribution is negligible. This is also noted in IEC 60891:2021,[35] where it is concluded that Procedure 2 is inappropriate for correcting irradiance below 600 W/m^2 to STC when the PV device has a low shunt resistance.

To conclude, the most influential environmental factor depends on the correction procedure. The effect of the irradiance *G* and the temperature *Tm* on RMSE is summarized in Table 3. Globally, there is one single dominant factor for one certain procedure under one certain condition. For the SC condition, the temperature *Tm* is a leading factor, whereas it is the irradiance *G* under the Rs degradation.

3.2 | Case studies for *I*–*V* curve correction

The impact of *G* and *Tm* on the RMSE under the five module conditions has been examined in detail. However, generally, not all the points in the *G*–*Tm* plane will be reached out in the field, like low *G*– high *Tm* or high *G*– low *Tm*. Therefore, to evaluate the correction procedures under real conditions, several case studies will be considered. They are obtained from simulated *I*–*V* curves with different environmental settings or fault severity tuned as follows:

- *Range of irradiance G*: The correction procedures have their own suitable application range of *G* for which the *I*–*V* curve is measured. Thus, the common measurable *G* is divided into three levels (defined in Table 4) to test the correction performance. The typical range is the high level as it is recommended to use *I*–*V* curves at high *G* to reduce correction error (Table 5).[32]
- *Season of measurement*: In the field, the correction of *I*–*V* curves may be done throughout the whole year, and the season has a significant impact on the measured *G* and *Tm*. Thus, this factor is also considered with the period of the seasons specified in Table 6. The default season is chosen as summer, where high *G* occurs more frequently, and PV modules have a higher output.

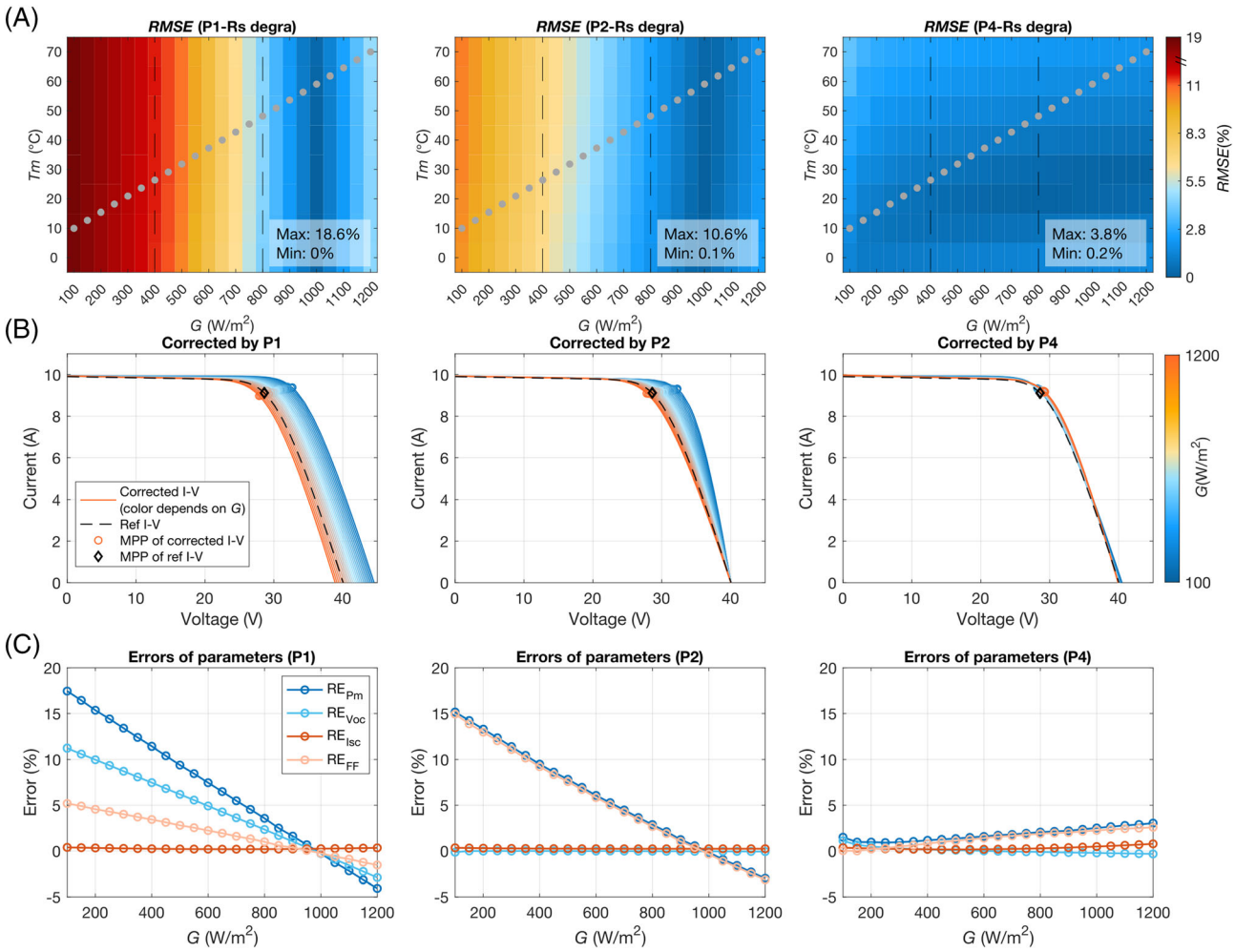

FIGURE 10 (A) Heatmap for the RMSE of the correction of *I*–*V* curves under Rs degradation using P1, P2, and P4 (gray points represent the *G* and *Tm* of example *I*–*V* curves, where the corrected ones and the related errors of parameters are shown in (B) and (C), respectively); (B) examples of corrected *I*–*V* curves under Rs degradation; and (C) errors of key parameters from the examples of corrected *I*–*V* curves [Colour figure can be viewed at wileyonlinelibrary.com]

- *Fault severity setting*: For PS, Rs, and Rsh degradation, when studying the impact of other factors, these fault severities will be set at typical values (Table 2). When analyzing the impact of fault severity, the values will vary in the ranges presented in Table 1.

The detailed configurations of the four case studies are displayed in Table 6.

To evaluate the correction procedures with real environmental conditions, *G* and *Tm* of the simulated curves are selected from on-site measurement of mc-Si PV modules in SIRTA meteorological and climate observatory (France).[44]

3.2.1 | Case 1: Using *I*–*V* curves at high-level *G* (summer) and constant fault severity

In this case, the *I*–*V* curves simulated at high-level *G* (illustrated in Figure 12) in summer are used for correction. The correction performance evaluation metrics (RMSE, RE_{P_m}, $RE_{V_{OC}}$, $RE_{I_{SC}}$, and RE_{FF}) are calculated and presented in Figure 13. It may be noted that the RMSE under these environmental conditions has already been presented in the heatmap in Section 3.1. The heatmap shows the qualitative trends while the results in Figure 13 provide a quantitative statistical presentation.

These performance metrics are analyzed as follows:

1. RMSE: The correction error on the whole curve is reflected by RMSE. The observations correspond to the previous results presented in Figure 6–11. Under PS and SC BPD, all three procedures introduce a large correction RMSE. Globally, P2 achieves better performance with the MAE of 2.6% compared to P1 (2.8%) and P4 (4.8%). The performance of P4, except under Rs degradation (the coefficient R_s is dynamically computed), is worse than the others, even under the healthy condition.
2. RE_{P_m}: P1 and P2 have similar correction performance, better than P4. Under PS and SC BPD, there is a significant positive error

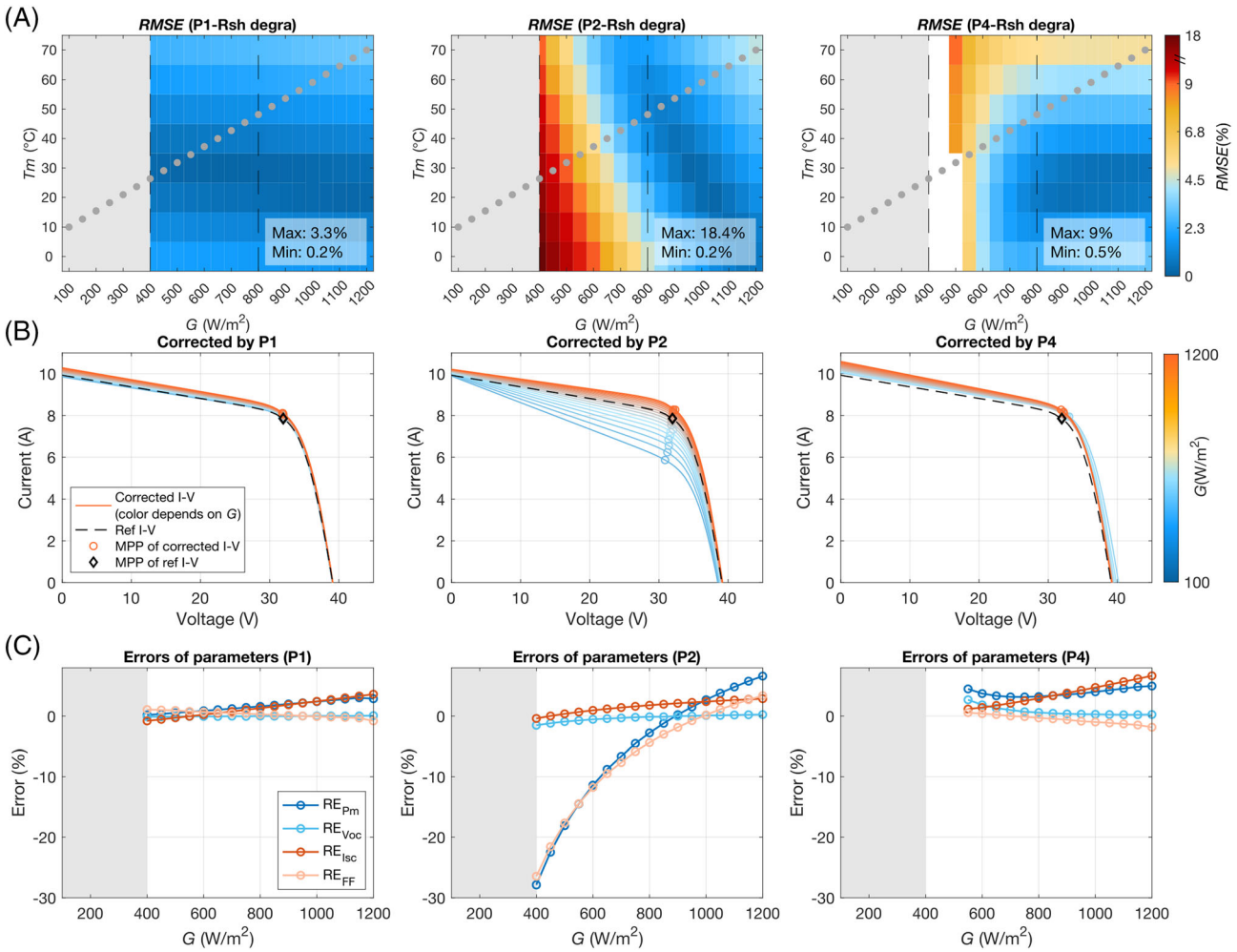

FIGURE 11 (A) Heatmap for the RMSE of the correction of *I–V* curves under Rsh degradation using P1, P2, and P4 (region when $G < 400$ W/m^2 are not tested since the *I–V* curves are greatly distorted due to the fault and low *G*; gray points represent the *G* and *Tm* of example *I–V* curves, where the corrected ones and the related errors of parameters are shown in (B) and (C), respectively); (B) examples of corrected *I–V* curves under Rsh degradation; and (C) errors of key parameters from the examples of corrected *I–V* curves [Colour figure can be viewed at wileyonlinelibrary.com]

TABLE 3 Influential environmental factors on correction procedures under five conditions

	Influential environmental factor		
Condition	**P1**	**P2**	**P4**
Healthy	*G*	*Tm*	*G* and *Tm*
PS	*G*	*Tm*	*G*
SC BPD	*Tm*	*Tm*	*Tm*
Rs degradation	*G*	*G*	*G*
Rsh degradation	*Tm*	*G*	*Tm*

TABLE 4 Three levels of *G*

Level	Range
High level	$G \geq 800$ W/m^2
Medium level	$400 \leq G < 800$ W/m^2
Low level	$G < 400$ W/m^2

TABLE 5 Period of seasons

Season	Period
Spring	Mars to May
Summer	June to August
Autumn	September to November
Winter	December to February

(up to 14.2% using P4) due to the distortions in the shape of the corrected curves (as shown in Figures 8 and 9). This means that the fault impact on P_m is underestimated, which may impede the detection of corresponding PV fault if P_m us used as fault signature.

3. $RE_{V_{OC}}$: Overall, P1 and P2 perform better V_{OC} correction compared to P4. However, under SC BPD conditions, all the procedures

TABLE 6 Configuration of case studies

Case	Season	Range of *G*	Fault severity
1	Summer	High level	Fixed
2	Summer	**Full range**	Fixed
3	**4 seasons**	High/medium* level	Fixed
4	Summer	High level	**Varying**

Note: The bold type is used to point out the range of variation to emulate each fault type.
*Due to there being very few data points at high-level *G* in winter, medium-level ones are added for evaluation.

generate an error of around 4.7% to 9.6%, which is, as discussed in Section 3.1, due to the use of an inappropriate voltage correction coefficient.

4. $RE_{I_{SC}}$: Except under Rsh degradation, $RE_{I_{SC}}$ is <0.7% for all the procedures. First, it should be noted that the corrected curve is usually shifted towards the right due to the voltage correction. Consequently, an extrapolation[45] is required to reach the current axis (*y* axis). In general, the slope is small near the I_{SC} region. However, in case of Rsh degradation, I_{MPP} is strongly reduced, which makes the slope steeper. Thus, the I_{SC} extracted from the corrected *I*–*V* curve deviates from the reference value (see Figure 11), which induces this large error.
5. RE_{FF}: As observed in Figure 8, due to the large correction bias of MPP under PS, the FF is greatly degraded with RE_{FF} up to 13.2%. In other conditions, RE_{FF} are relatively lower. Globally, P1 and P2 present similar and better correction of FF than P4.

3.2.2 | Case 2: Using *I*–*V* curves over the full range of irradiance *G* (summer) and constant fault severity

For this case, the correction of curves simulated with low and medium values of irradiance *G* (shown in Figure 12) is also tested. RMSE and RE_{P_m} are calculated and presented in Figure 14. For Rsh degradation the results are not displayed, since the corrected *I*–*V* curves for low *G* are greatly distorted or fail to be corrected.

Regarding the RMSE over the total range of variation for *G*, the results correspond to the influential factors listed in Table 3. For the procedure more sensitive to *G* than to the temperature *Tm*, a decreasing trend of RMSE could be observed with increasing *G*, like P1 and P4 under healthy, PS, and Rs degradation. Conversely, if *Tm* is the dominant factor, a higher *G* will lead to a higher *Tm*, resulting in higher RMSE. Thus, RMSE increases with *G*, like all the procedures under SC BPD. It should be noted that none of the procedures is better over the whole range of variation. P2 performs better in healthy and PS conditions while P1 in SC BPD and Rsh degradation.

As for RE_{P_m}, the trend is broadly similar to RMSE. It should be noted that RE_{P_m} is not an absolute value metric like RMSE. When RE_{P_m} is positive, it means the P_m is underestimated and vice versa. Except under the healthy condition, RE_{P_m} is quite large (higher than

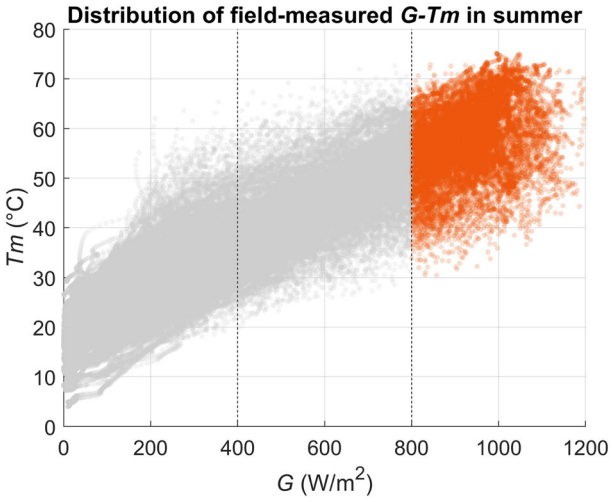

FIGURE 12 Distribution of *G*–*Tm* in summer (data points with high-level *G* are marked in orange) [Colour figure can be viewed at wileyonlinelibrary.com]

10%). Even worse, catastrophic misestimation can be caused by using P1 (45.5%) and P4 (up to 72.4%) under PS for low values of *G*.

3.2.3 | Case 3: Using *I*–*V* curves at high/medium-level *G* (four seasons) and constant fault severity

Hereafter, the impact of the season on the correction procedures is investigated. To ensure a fair comparison for the four seasons, *I*–*V* curves simulated for medium-level *G* are merged with the ones at high-level *G* for the evaluation of the correction because there are very few data points recorded at high-level *G* in winter (as shown in Figure 15).

Similarly, the curve RMSE and RE_{P_m} for the four seasons are calculated and presented in Figure 16.

For the RMSE, overall, the performance using the spring and autumn *I*–*V* curves is similar since the distributions of *G* and *Tm* are similar, as shown in Figure 15. For summer and winter, different trends are observed. Because the *I*–*V* curves in winter are at much lower *Tm* than in summer (about 20°C lower on average, as shown in Figure 15), if the RMSE is more sensitive to high *Tm*, the error will be higher in summer than in winter, as P2 and P4 in healthy and SC BPD conditions. Conversely, if the RMSE is more sensitive to high *G*, the RMSE in winter will increase compared to summer, as P1 in PS and Rs degradation. Still, none of the three procedures outperform for all the conditions. P2 exhibits better performance for healthy and PS while P1 in SC BPD and Rsh degradation. P4 is only competitive under Rs degradation.

Concerning RE_{P_m}, overall, the trend agrees with that of RMSE. The performance during spring, summer, and fall are relatively stable due to the similar distribution of *G* and *Tm*. Depending on the sensitivity to *G* and *Tm* as discussed above, RE_{P_m} in winter either shows the lowest or the largest error, while the large error could reach 24.8% using P4 and 20.6% using P1 under PS, and −14.5% in the case of Rsh degradation using P2.

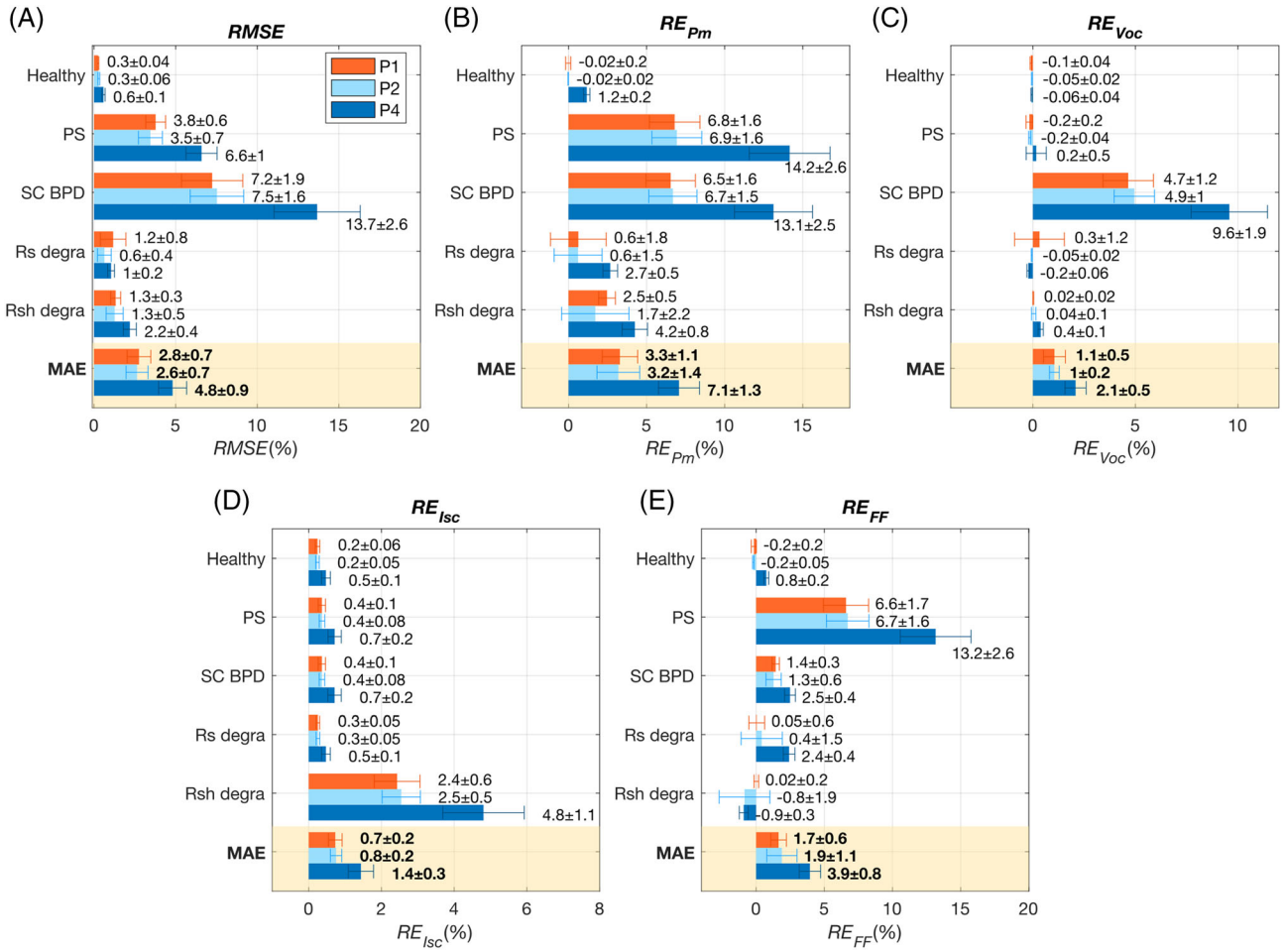

FIGURE 13 Correction performance of P1, P2, and P4 in Case 1: (A) RMSE, (B) RE_{P_m}, (C) $RE_{V_{OC}}$, (D) $RE_{I_{SC}}$, and (E) RE_{FF} (the bars refer to the mean value, and horizontal whiskers represent the standard deviation (std), these two values are marked as "mean" ± "std"; the mean absolute error (MAE) of the six conditions is also presented) [Colour figure can be viewed at wileyonlinelibrary.com]

3.2.4 | Case 4: Using *I*–*V* curves with high-level *G* (summer) and varying fault severity

While the previous cases studied the effect of environmental parameters, this one will allow evaluating the effect of the severity of the defect. The severities of PS, Rs, and Rsh degradations are varied in the ranges presented in Table 1, while the level of irradiance is set to high-level summer values as in Case 1. E_{curve} and RE_{P_m} calculated from these corrected curves are presented in Figure 17 as a function of the fault severity.

Based on Figure 17, several remarks can be drawn:

- Both RMSE and RE_{P_m} show an increasing trend with the fault severities. They are more sensitive to PS and severe Rsh degradation;
- A step variation on RE_{P_m} is observed for PS, which is due to the unsynchronized shifting of maximum power point (MPP) between corrected and reference curves as illustrated in Figure 18;
- Under PS, when the PS degree is too large, the current of the reflection point decreases (also seen from Figures 3 and 18). In these cases, P4 is no more applicable since there are few points in the high-voltage steep curve area to extract Rs based on the standard.[35]
- Overall, the performance of P2 is better than P1 and P4.
- RE_{P_m} is nearly all positive for all procedures. This means that the correction leads to an underestimation of the impact of the fault on P_m. Moreover, this underestimation increases with the severity of the fault. This is troublesome if P_m is used as an indicator of the health of the PV generator.

3.3 | Preliminary test on field *I*–*V* curves

To evaluate the performance of these procedures on the actual data, field-measured *I*–*V* curves of the same PV sc-Si module are measured for tests. The measurement configuration is presented in Section 2.1.2.

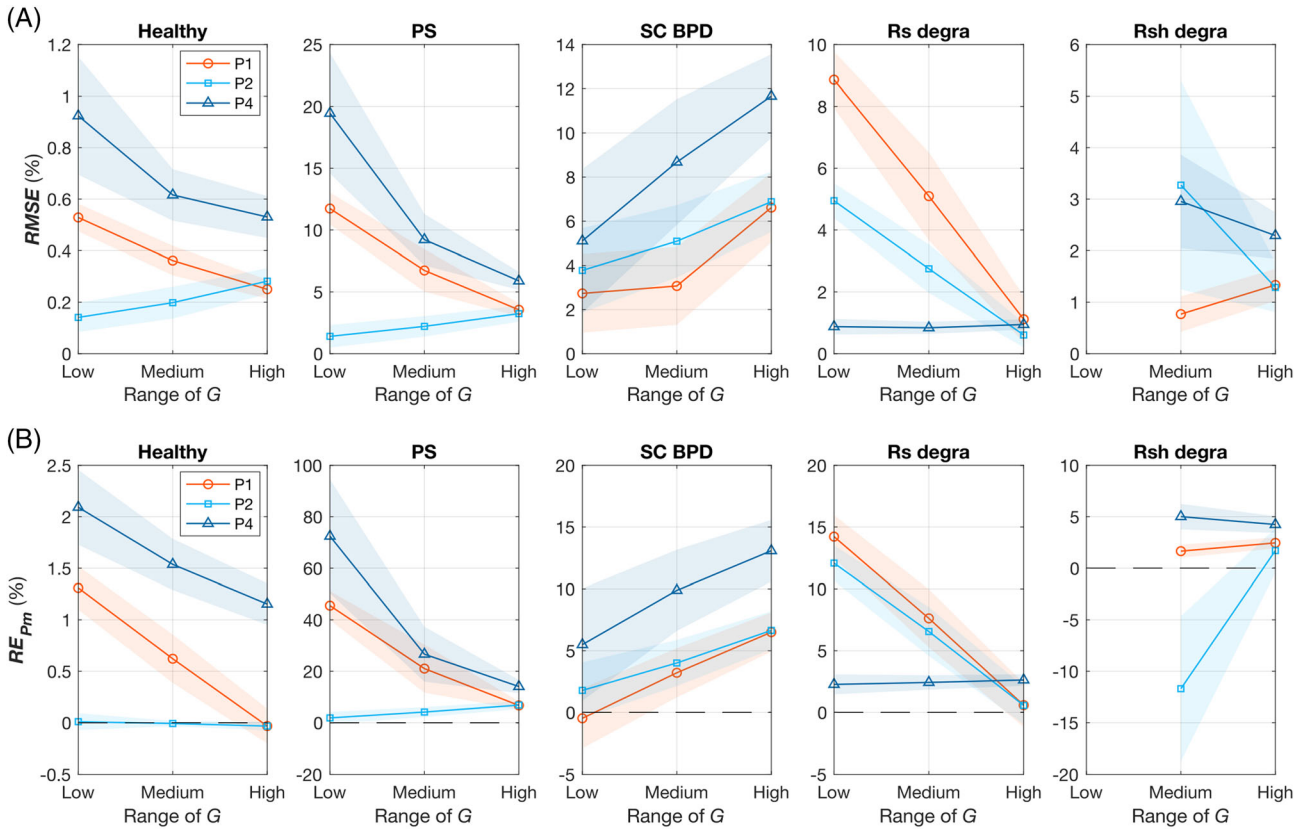

FIGURE 14 Correction performance of P1, P2, and P4 in Case 2: (A) RMSE, (B) RE_{P_m} (the marked line refers to the mean value and band area represents the std) [Colour figure can be viewed at wileyonlinelibrary.com]

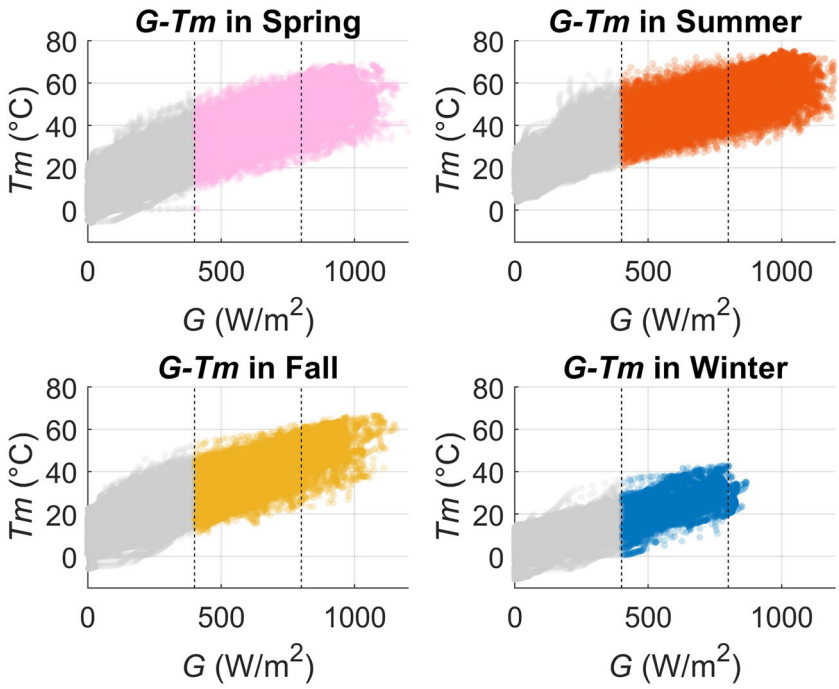

FIGURE 15 Distribution of field-measured *G–Tm* of the four seasons (data points with medium and high-level *G* are marked in color) [Colour figure can be viewed at wileyonlinelibrary.com]

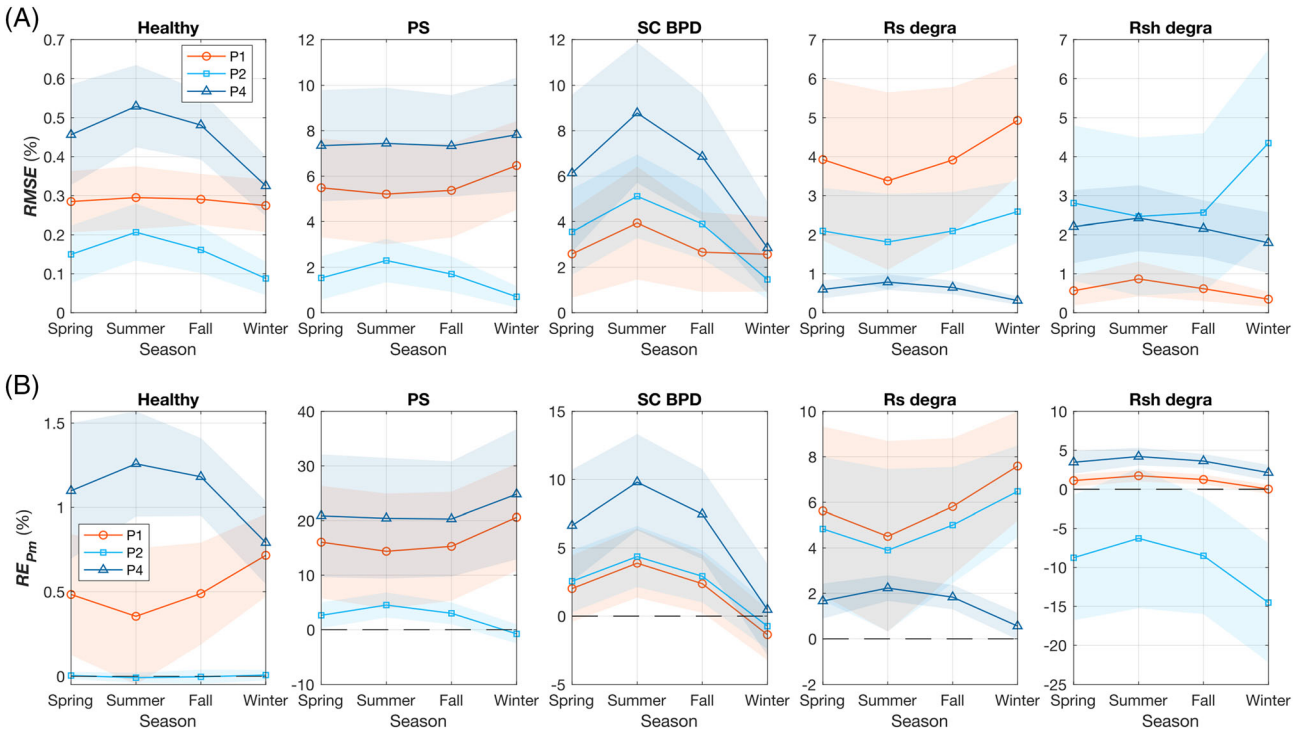

FIGURE 16 Correction performance of P1, P2, and P4 in Case 3: (A) RMSE and (B) RE_{P_m} (the marked line refers to the mean value and band area represents the std) [Colour figure can be viewed at wileyonlinelibrary.com]

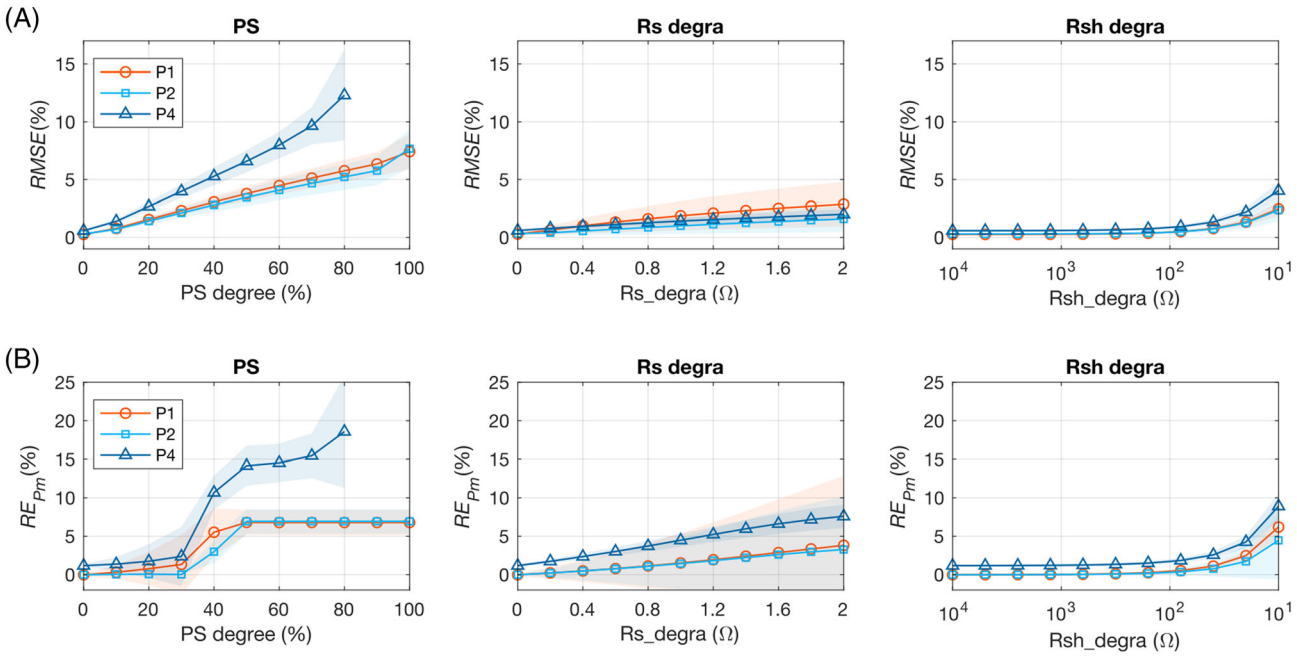

FIGURE 17 Correction performance of P1, P2, and P4 in Case 4: (A) *RMSE* and (B) RE_{P_m} (the marked line refers to the mean value and band area represents the std; the module condition is presented from healthy to severe on the *x* axis from left to right; under PS, P4 is not applicable when PS degree is larger than 80%) [Colour figure can be viewed at wileyonlinelibrary.com]

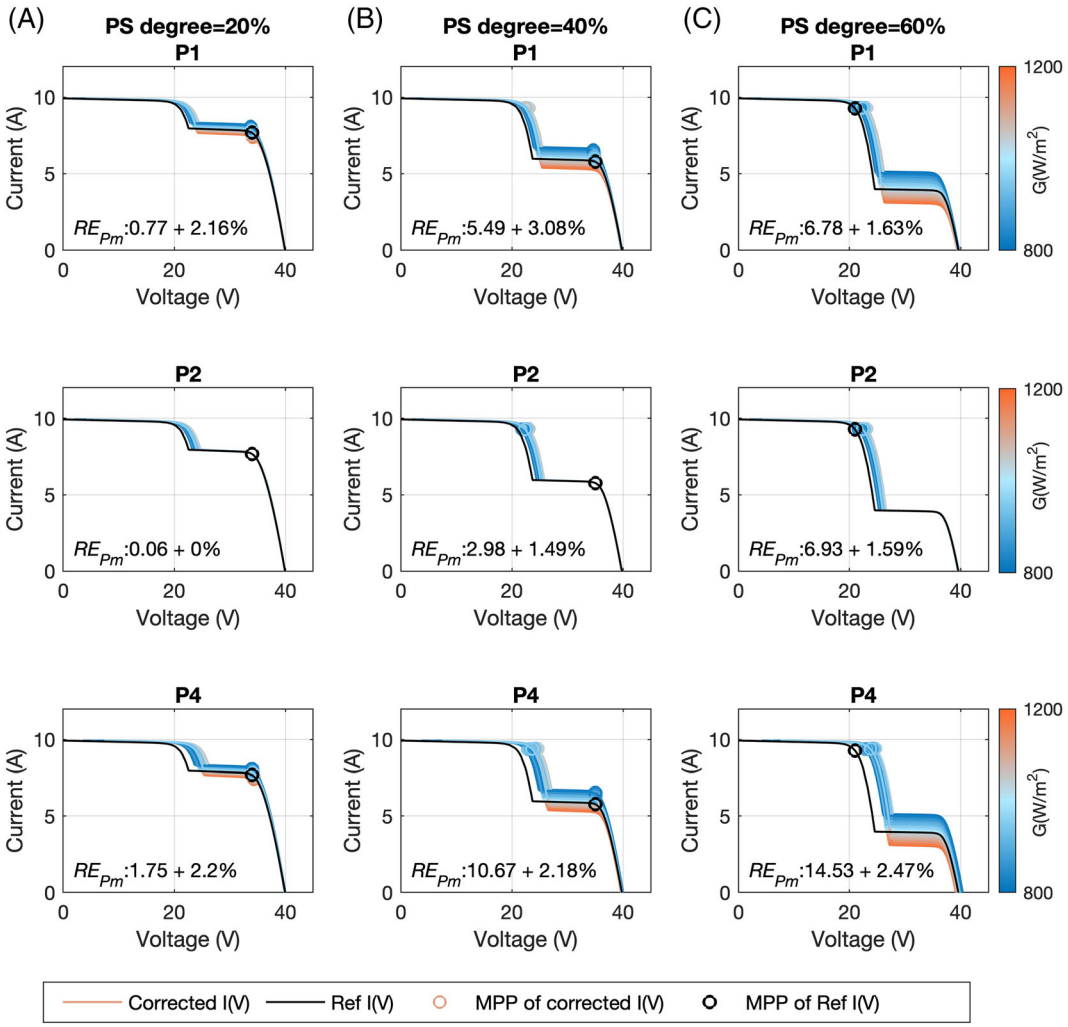

FIGURE 18 Corrected curves and RE_{P_m} using P1, P2, and P4 under three fault severities of PS: (A) PS degree = 20%, (B) PS degree = 40%, (C) PS degree = 60% (the color of corrected curves depends on *G*; RE_{P_m} is presented as "mean + std") [Colour figure can be viewed at wileyonlinelibrary.com]

3.3.1 | Limits of the field test

It should be noted that it is challenging to perform a quantitative and non-bias evaluation of correction using field data for all the conditions studies as in Sections 3.1 and 3.2 due to the following limits:

- Measurement uncertainty: Although the measurement devices are routinely calibrated, the measurement uncertainty for the *I*–*V* curve, irradiance, and temperature could still be up to 1–2%. This uncertainty, in certain cases, is far above the RMSE caused by the correction procedure. Thus, we cannot fully contribute the observed error using the real *I*–*V* curves to the correction procedures.
- Lack of reference curve: The module is fixed in the rack for continuous measurement and the current condition does not allow to move it and carry on the in-door high-quality flash test to get the *I*–*V* curve of the current condition at precise STC.
- Lack of curves under faulty conditions: Currently, the module is occupied for a project of long-term health monitoring research. It is not permitted to produce manual PV faults on the module, like SC BPD and abnormal degradation.

Despite these limits, we can still apply the correction procedures to the real *I*–*V* curves. Specifically, the measured *G* and *Tm* are used to correct the recorded *I*–*V* curves. The *I*–*V* curve produced from datasheet information at STC is adopted as the reference curve to quantify the mismatch. It should be noted that, due to the limits, although the calculated errors do not reflect the absolute correction error caused by the procedures, they can provide insight into the relative comparison among the three procedures.

3.3.2 | Correction performance

After data cleaning and filtering, 659 *I*–*V* curves measured during summer and at high *G* level ($G \geq 800$ W/m^2) are corrected with the results shown in Figure 19.

Globally, the curve RMSE and errors of parameters are all larger than those obtained from the simulation study, which is logical since the presence of the three limits of the field test as explained in Section 3.3.1. As for the three procedures, they exhibit similar performance using the curves under the healthy condition, which corresponds to the results presented in Figure 13. Comparatively, P2 achieves better performance with the lowest RMSE and RE_{P_m}. In addition, P2 has a lower variation for most error metrics, which demonstrates the higher robustness of the correction.

4 | DISCUSSION

4.1 | Summary of correction procedures

The correction performance with P1, P2, or P4 has been evaluated for several environmental and different fault conditions and severity. Each procedure has its advantages and disadvantages, as summarized in Table 7.

None of the three procedures performs well under all conditions, considering the variation of seasons, irradiance level, and severity of defects. However, if the condition of the PV module can be roughly estimated, it is possible to select a correction procedure, as shown in Table 8. It should be noted that PS and SC BPD are relatively severe defects in the PV module, which can lead to significant distortion of the *I*–*V* curves. Therefore, these faults are usually easily detected, even from the *I*–*V* curves before correction. In comparison, the impact of the degradation of Rs or Rsh on the *I*–*V* curve is relatively limited, especially when the degradation is in the initial stage. In these cases, the correction of the *I*–*V* curve is even more justified.

Overall, P2 is a reasonable choice for most conditions, especially for *I*–*V* curves measured at high-level *G*, which is also validated using field-measured *I*–*V* curves. However, it should be noted that under Rsh degradation and for low irradiance, the correction performance is greatly deteriorated, as it has been observed from Figures 11 and 14. P1 is very similar to P2, but with lower performance. Regarding P4, although free of prior-determined correction coefficients, it exhibits the lowest performance, almost under all conditions. Finally, the selection of the procedure is a compromise between the correction performance and the complexity.

TABLE 8 Suggested correction procedure under specific module conditions

PV module condition	Suggested procedure
Healthy	P2
PS	P2
SC BPD	P1/P2
Rs degradation	P4
Rsh degradation	P1

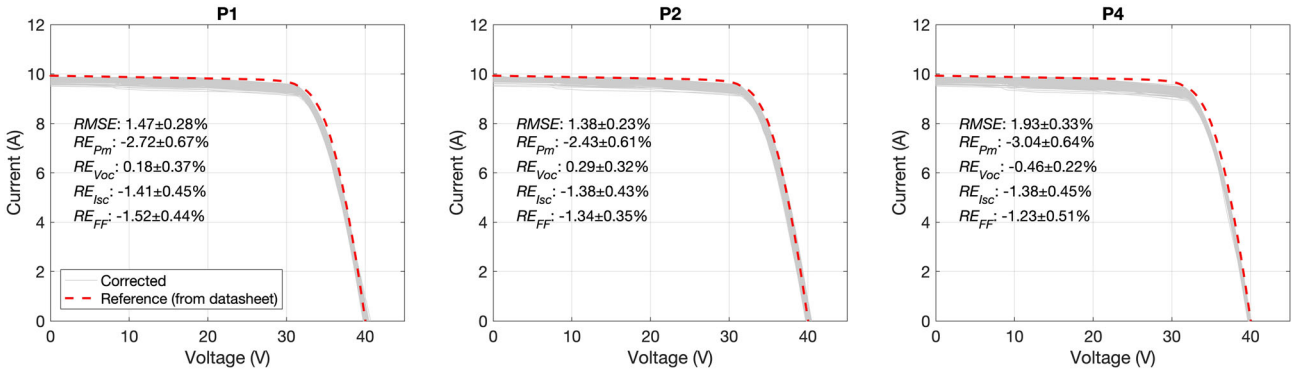

FIGURE 19 Corrected field-measured *I*–*V* curves using P1, P2, and P4 [Colour figure can be viewed at wileyonlinelibrary.com]

TABLE 7 Pros and cons of correction procedure

	P1	P2	P4
Pros	• Simplicity compared to P2	• Best performance in most conditions • Insensitive to seasons • Robust to varying fault severity	• Free of prior-determined correction coefficients • Dynamical determination of Rs coefficient
Cons	• Requirement to determine two correction coefficients (R_s, κ) • Catastrophic correction under PS	• Requirement to determine four correction coefficients (R_s', κ', B_1, B_2) • Poor correction under Rsh degradation	• Usually fail to perform at low irradiance • Catastrophic correction under PS

4.2 | Challenges and prospects

From the previous analyses, several challenges have been identified. First, for P1 and P2, there is a need to determine several correction coefficients based on a group of *I*–*V* curves at the same *G* or same *Tm*, which is troublesome and time-consuming, especially for on-site applications. Second, the correction coefficients computed from simulated data may not conform well to the actual values in the field, especially for the aging or faulty PV modules. In addition, the correction performance for all the procedures (reflected from the shape of the curve and P_m) is still poor under several conditions, like PS, short-circuited bypass diode, and Rsh degradation. Lastly, for the validation on field tests, there are still several limits that impede a precise evaluation of the correction performance, like measurement uncertainty, lack of reference and faulty curves.

Hereafters are some prospective works to improve the standard procedures. The methods to compute the correction coefficients should be adapted for field application. When the *G* and *Tm* of the measured *I*–*V* curves are close but do not perfectly match the values at STC, a compensation method should be introduced. Also, it is suggested to determine more coefficients dynamically based on the curve to correct, as P4 computes the Rs coefficient. This will reduce the dependence on prior-determined correction coefficients. Finally, the procedures should be adapted to achieve similar performance whatever the PV module health conditions.

5 | CONCLUSION

The *I*–*V* curves correction procedures proposed in the IEC 60891:2021 standard have been evaluated with data measured from an mc-Si PV module under healthy and defective conditions. The impact of environmental factors on the curve correction error has been investigated. Each procedure may be more sensitive to either irradiance or module temperature under different conditions. Four special study cases have been considered with an emphasis on the season of measurement, the range of irradiance values, and the fault severity. It has been shown that a distortion of the curve shape is usually introduced by the correction procedures, which will consequently lead to the misestimation of key curve parameters. Notably, for the maximum power P_m, an underestimation is observed with a *RE* up to 14.2%. This may greatly hinder the detection of PV faults if P_m is used as the fault indicator.

It has also been found that none of the three procedures outperforms under all the conditions. However, overall, Procedure 2 exhibits higher performance with the relative root-mean-square error of the curve current as 2.6% compared to Procedure 1 (2.8%) and Procedure 4 (4.8%). Experimental tests using real *I*–*V* curves also demonstrate that Procedure 2 exhibits better robustness of correction. Nevertheless, its performance under Rs and Rsh degradation is still poor. For Procedure 4, the performance under PS or short-circuit bypass conditions is the weakest. Nevertheless, it shows similar or better performance than Procedures 1 and 2 for faults that are generally less easily detected and for which *I*–*V* correction is more than necessary. In this respect, Procedure 4 is a promising alternative correction method when precisely predetermined correction coefficients are unavailable.

The *I*–*V* curve correction is essential to many *I*–*V* curve-based PV health monitoring and fault diagnosis. Therefore, it is of great importance to ensure both good correction accuracy and easy implementation. To this end, several future works are expected: adapt the correction procedure to on-site application, dynamically determine the correction coefficients, and develop a correction procedure adapted to different faulty conditions.

ACKNOWLEDGEMENT

The authors would like to acknowledge the SIRTA for the on-site data.

DATA AVAILABILITY STATEMENT

The data that support the findings of this study are available from the corresponding author upon reasonable request.

NOMENCLATURE

a	irradiance correction factor
BPD	bypass diode
EL	electroluminescence
G	global plane of Array irradiance (W/m^2)
I	current (A)
I_{MPP}	current at maximum power point (A)
I_{SC}	short-circuit current (A)
I–*V* curve	current–voltage characteristics
MPP	maximum power point
n	diode factor
OC	open circuit
P_m	maximum power (W)
PS	partial shading
PV	photovoltaic
RE	relative error (%)
RMSE	root-mean-square error
R_{OC}	resistance used in simulation for OC (Ω)
R_s	series resistance (Ω)
R_{s_degra}	resistance used in simulation for Rs degradation (Ω)
R_{SC}	resistance used in simulation for SC (Ω)
R_{sh}	shunt resistance (Ω)
R_{sh_degra}	resistance used in simulation for Rsh degradation (Ω)
SC	short circuit
STC	standard test condition
TC	temperature coefficient
Tm	module temperature (°C)
V	voltage (V)
V_{MPP}	voltage at MPP (V)
V_{OC}	open-circuit voltage (V)
VDTC	voltage-dependent temperature coefficient
α	absolute temperature coefficient of I_{SC} (A/°C)
α_{rel}	relative temperature coefficient of I_{SC} (%/°C)

β	absolute temperature coefficient of V_{OC} (V/°C)
β_{rel}	relative temperature coefficient of V_{OC} (%/°C)
κ	curve correction factor

ORCID

Demba Diallo https://orcid.org/0000-0002-4421-6175
Claude Delpha https://orcid.org/0000-0003-3224-8628

REFERENCES

1. Muller M, Kurtz S, Steiner M, Siefer G. Translating outdoor CPV *I–V* measurements to a CSTC power rating and the associated uncertainty. *Prog Photovolt: Res Appl*. 2015;23:1557-1571. doi:10.1002/PIP.2590
2. Li B, Delpha C, Migan-Dubois A, Diallo D. Fault diagnosis of photovoltaic panels using full I–V characteristics and machine learning techniques. *Energ Conver Manage*. 2021;248:114785. doi:10.1016/J.ENCONMAN.2021.114785
3. Huang JM, Wai RJ, Gao W. Newly-designed fault diagnostic method for solar photovoltaic generation system based on IV-curve measurement. *IEEE Access*. 2019;7:70919-70932. doi:10.1109/ACCESS.2019.2919337
4. Chen Z, Wu L, Cheng S, Lin P, Wu Y, Lin W. Intelligent fault diagnosis of photovoltaic arrays based on optimized kernel extreme learning machine and I-V characteristics. *Appl Energy*. 2017;204:912-931. doi:10.1016/j.apenergy.2017.05.034
5. Agrawal N, Bora B, Kapoor A. Experimental investigations of fault tolerance due to shading in photovoltaic modules with different interconnected solar cell networks. *Solar Energy*. 2020;211:1239-1254. doi:10.1016/j.solener.2020.10.060
6. Wang M, Liu J, Burleyson TJ, et al. Analytic I_{sc}–V_{oc} method and power loss modes from outdoor time-series *I–V* curves. *IEEE J Photovolt*. 2020;10:1379-1388. doi:10.1109/JPHOTOV.2020.2993100
7. Jordan DC, Silverman TJ, Sekulic B, Kurtz SR. PV degradation curves: non-linearities and failure modes. *Prog Photovolt: Res Appl*. 2017;25(7):583-591. doi:10.1002/PIP.2835
8. Silva AM, Melo FC, Reis JH, Freitas LCG. The study and application of evaluation methods for photovoltaic modules under real operational conditions, in a region of the Brazilian Southeast. *Renew Energy*. 2019;138:1189-1204. doi:10.1016/j.renene.2019.01.129
9. IEC 60891. Photovoltaic devices—procedures for temperature and irradiance corrections to measured I-V characteristics. 2009.
10. Bouaichi A, Alami A, Hajjaj C, et al. In-situ evaluation of the early PV module degradation of various technologies under harsh climatic conditions: the case of Morocco. *Renew Energy*. 2019;143:1500-1518. doi:10.1016/j.renene.2019.05.091
11. Rajput P, Tiwari GN, Sastry OS, Bora B, Sharma V. Degradation of mono-crystalline photovoltaic modules after 22 years of outdoor exposure in the composite climate of India. *Solar Energy*. 2016;135:786-795. doi:10.1016/j.solener.2016.06.047
12. Golive YR, Singh HK, Kottantharayil A, Vasi J, Shiradkar N. Investigation of accuracy of various STC correction procedures for I-V characteristics of PV modules measured at different temperature and irradiances. In: *2019 IEEE 46th Photovoltaic Specialists Conference (PVSC)*. IEEE; 2019:2743-2748. doi:10.1109/PVSC40753.2019.8980557
13. Dolara A, Lazaroiu GC, Leva S, Manzolini G. Experimental investigation of partial shading scenarios on PV (photovoltaic) modules. *Energy*. 2013;55:466-475. doi:10.1016/j.energy.2013.04.009
14. Fadhel S, Diallo D, Delpha C, et al. Maximum power point analysis for partial shading detection and identification in photovoltaic systems. *Energ Conver Manage*. 2020;224:113374. doi:10.1016/j.enconman.2020.113374
15. Ma M, Liu H, Zhang Z, Yun P, Liu F. Rapid diagnosis of hot spot failure of crystalline silicon PV module based on I-V curve. *Microelectron Reliab*. 2019;100–101:113402. doi:10.1016/j.microrel.2019.113402
16. Tanesab J, Parlevliet D, Whale J, Urmee T, Pryor T. The contribution of dust to performance degradation of PV modules in a temperate climate zone. *Solar Energy*. 2015;120:147-157. doi:10.1016/j.solener.2015.06.052
17. Tanesab J, Parlevliet D, Whale J, Urmee T. Seasonal effect of dust on the degradation of PV modules performance deployed in different climate areas. *Renew Energy*. 2017;111:105-115. doi:10.1016/j.renene.2017.03.091
18. Martínez-Moreno F, Figueiredo G, Lorenzo E. In-the-field PID related experiences. *Sol Energy Mater Sol Cells*. 2018;174:485-493. doi:10.1016/j.solmat.2017.09.037
19. Piliougine M, Oukaja A, Sánchez-Friera P, et al. Analysis of the degradation of single-crystalline silicon modules after 21 years of operation. *Prog Photovolt: Res Appl*. 2021;29(8):907-919. doi:10.1002/PIP.3409
20. Kahoul N, Cheghib H, Sidrach-de-Cardona M, Affari BC, Younes M, Kherici Z. Performance degradation analysis of crystalline silicon solar cells in desert climates. *Energy Sustain Dev*. 2021;65:189-193. doi:10.1016/J.ESD.2021.10.010
21. Martínez JF, Steiner M, Wiesenfarth M, Siefer G, Glunz SW, Dimroth F. Power rating procedure of hybrid concentrator/flat-plate photovoltaic bifacial modules. *Prog Photovolt: Res Appl*. 2021;29(6):614-629. doi:10.1002/PIP.3410
22. Raina G, Vijay R, Sinha S. Assessing the suitability of I-V curve translation at varying irradiance and temperature range. *Sustain Energy Technol Assess*. 2022;51:101925. doi:10.1016/J.SETA.2021.101925
23. Wilking S, Ebert S, Beckh C, Herguth A, Hahn G. Precise determination of the STC I-V curves by wide-range linear extrapolation of outdoor I-V curves on partly sunny days. In: *32nd European Photovoltaic Solar Energy Conference and Exhibition*. WIP; 2016:1716-1719. doi:10.4229/EUPVSEC20162016-5DO.11.4
24. Kumar V, Maheshwari P. Advanced analytics on IV curves and electroluminescence images of photovoltaic modules using machine learning algorithms. *Prog Photovolt: Res Appl*. 2022;30(8):880-888. doi:10.1002/PIP.3469
25. Ayang A, Wamkeue R, Ouhrouche M, et al. Least square estimator and IEC-60891 procedure for parameters estimation of single-diode model of photovoltaic generator at standard test conditions (STC). *Electr Eng*. 2021;103(2):1253-1264. doi:10.1007/S00202-020-01131-2/FIGURES/10
26. Dobreva P, van Dyk EE, Vorster FJ. Irradiance and temperature corrections of current-voltage curves—quintessential nature and implications. *Solar Energy*. 2021;227:116-125. doi:10.1016/J.SOLENER.2021.08.057
27. Duck BC, Fell CJ, Marion B, Emery K. Comparing standard translation methods for predicting photovoltaic energy production. In: *Conference Record of the IEEE Photovoltaic Specialists Conference*. IEEE; 2013:763-768. doi:10.1109/PVSC.2013.6744261
28. Haas S, Bauer A, Lambertz A, Rau U. Assessment of STC conversion methods under outdoor test conditions. In: *26th European Photovoltaic Solar Energy Conference and Exhibition*. WIP; 2011:3458-3462. doi:10.4229/26THEUPVSEC2011-4AV.1.52
29. Tsuno Y, Hishikawa Y. Comparison of curve correction procedures for current-voltage characteristics of photovoltaic devices. *Jpn J Appl Phys*. 2012;51(10S):10NF02. doi:10.1143/JJAP.51.10NF02/XML
30. Padilla A, Londoño C, Jaramillo F, Tovar I, Cano JB, Velilla E. Photovoltaic performance assess by correcting the I-V curves in outdoor tests. *Solar Energy*. 2022;237:11-18. doi:10.1016/J.SOLENER.2022.03.064
31. Paudyal BR, Imenes AG. Investigation of temperature coefficients of PV modules through field measured data. *Solar Energy*. 2021;224:425-439. doi:10.1016/J.SOLENER.2021.06.013

32. Ding K, Zhang J, Bian X, Xu J. A simplified model for photovoltaic modules based on improved translation equations. *Solar Energy*. 2014;101:40-52. doi:10.1016/J.SOLENER.2013.12.016
33. Golive YR, Kottantharayil A, Vasi J, Shiradkar N. Determining the optimal standard test condition correction procedure for high-throughput field I–V measurements of photovoltaic modules. *Prog Photovolt: Res Appl*. 2022;30:13-26. doi:10.1002/PIP.3457
34. Abe CF, DIas JB, Haeberle F, Notton G, Faggianelli GA. Simplified approach to adjust IEC-60891 equation coefficients from experimental measurements with long-term validation. *IEEE J Photovolt*. 2021;11(2):496-503. doi:10.1109/JPHOTOV.2020.3043101
35. IEC 60891. Photovoltaic devices—procedures for temperature and irradiance corrections to measured I-V characteristics. 2021.
36. Pingel S, Erath D, Wenzel T, et al. I-V translation procedure for higher accuracy and compliance with PERC cell technology requirements. In: *37th European Photovoltaic Solar Energy Conference and Exhibition*. WIP; 2020:1120-1125. doi:10.4229/EUPVSEC20202020-4AV.2.19
37. Hishikawa Y, Takenouchi T, Higa M, Yamagoe K, Ohshima H, Yoshita M. Translation of solar cell performance for irradiance and temperature from a single I-V curve without advance information of translation parameters. *IEEE J Photovolt*. 2019;9(5):1195-1201. doi:10.1109/JPHOTOV.2019.2924388
38. Golive YR, Kottantharayil A, Shiradkar N. Sensitivity of accuracy of various standard test condition correction procedures to the errors in temperature coefficients of c-Si PV modules. *Prog Photovolt: Res Appl*. 2022;30(9):1087-1100. doi:10.1002/PIP.3559
39. Piliougine M, Sánchez-Friera P, Petrone G, Sánchez-Pacheco FJ, Spagnuolo G, Sidrach-de-Cardona M. Analysis of the degradation of amorphous silicon-based modules after 11 years of exposure by means of IEC60891:2021 procedure 3. *Prog Photovolt: Res Appl*. 2022;30(10):1176-1187. doi:10.1002/PIP.3567
40. Li B, Migan-Dubois A, Delpha C, Diallo D. Evaluation and improvement of IEC 60891 correction methods for I-V curves of defective photovoltaic panels. *Solar Energy*. 2021;216:225-237. doi:10.1016/j.solener.2021.01.010
41. Li B, Migan-Dubois A, Delpha C, Diallo D. Analysis of the performance of I-V curve correction methods in the presence of defects. In: *37th European Photovoltaic Solar Energy Conference and Exhibition (EU PVSEC), Virtual Conference*. EU PVSEC; 2020:1599-1603. doi:10.4229/EUPVSEC20202020-5CV.3.54
42. de Soto W, Klein SA, Beckman WA. Improvement and validation of a model for photovoltaic array performance. *Solar Energy*. 2006;80(1):78-88. doi:10.1016/J.SOLENER.2005.06.010
43. Hishikawa Y, Doi T, Higa M, et al. Voltage-dependent temperature coefficient of the I-V curves of crystalline silicon photovoltaic modules. *IEEE J Photovolt*. 2018;8(1):48-53. doi:10.1109/JPHOTOV.2017.2766529
44. Migan A, Mambrini T, Bourdin V, Badosa J. Deployment of a multi-technology photovoltaic module test bench on the SIRTA meteorological and climate observatory. In: *31st European PV Solar Energy Conference and Exhibition (EU PVSEC)*. WIP; 2015.
45. Bühler AJ, Perin Gasparin F, Krenzinger A. Post-processing data of measured I–V curves of photovoltaic devices. *Renew Energy*. 2014;68:602-610. doi:10.1016/j.renene.2014.02.048

SUPPORTING INFORMATION

Additional supporting information can be found online in the Supporting Information section at the end of this article.

How to cite this article: Li B, Diallo D, Migan-Dubois A, Delpha C. Performance evaluation of IEC 60891:2021 procedures for correcting *I–V* curves of photovoltaic modules under healthy and faulty conditions. *Prog Photovolt Res Appl*. 2022;1-20. doi:10.1002/pip.3652